CNRS
Centre National de la Recherche Scientifique

INFN
Instituto Nazionale di Fisica Nucleare

VSR2 mirror and marionette actuator calibration

L. Rolland

VIR-0076B-10

February 5, 2010

VIRGO * A joint CNRS-INFN Project
Project office: Traversa H di via Macerata - I-56021 S. Stefano a Macerata, Cascina (PI)
Secretariat: Telephone (39) 50 752 521 – Fax (39) 50 752 550 – e-mail virgo@pisa.infn.it

Contents

1 Introduction

This note gives the status of the Virgo mirror and marionette actuator calibration using all the VSR2 data, including the pre- and post-VSR2 data, from June 2009 to January 2010.

The calibration of the dark fringe sensing for VSR2 (including some timing studies) is described in the first section of the note VIR-0576A-09 [1] from October 2009. Some details were also given in the note appendix.
In the present note, the sections 3 and 4 about the actuation calibration have been updated. Section 5 has been added in order to compare the parameterizations used for the VSR2 hardware injections to the final actuation model.

During the run VSR2, some data were taken every weeks or two weeks with the same configurations each time in order to monitor the parameter stability. Before and after the run, additionnal measurements were done in order to improve the calibration precision and understanding.

The calibration period is from GPS 930000000 to 948000000.

2 Dark fringe sensing

Nothing changed since note VIR-0576A-09 from October 2009.

The tables with the models of the sensing are given again such that all the calibration parameterizations are included in this note.

The shape of the digital 8th order Butterworth filter used in the ADC of dark fringe readout at 20 kHz is shown in the figure 1.

2.1 Tables

Parameters	Full model ($f < 20\,\mathrm{kHz}$)	Simple model ($f < 2\,\mathrm{kHz}$)
Gain	1	1
Φ_0 (rad)	0	0
Delay (μs)	-59.7	49.3
Butterworth frequency (Hz)	7503.65	–

Table 1: ***Models for the sensing of the*** $Pr\_B1\_\{d2, d3\}$***,*** Pr_B1 ***and*** $Pr\_B1p\_\{d1, d2\}$ ***channels at 20 kHz.*** *The delays are given related to the absolute GPS time.* **Simple model***: the delay has been measured with the ramped 1 PPS. It is valid up to 2 kHz.* **Full model***: the delay is the simple model delay subtracted for the Butterworth equivalent delay. It is valid up to 20 kHz. Systematic errors are* ± 4 μs *on the delay.*

Parameters	$Pr\_B1\_d2\_ACp\_40K$	$Pr\_B1\_d3\_ACp\_40K$
Gain	1	1
Φ_0 (rad)	0	0
Delay (μs)	-32.28 ± 0.0001	-32.16 ± 0.0001
8th order Butterworth frequency (Hz)	15007.30	15007.30
Zero frequency (Hz)	2.38939 ± 0.00011	2.37568 ± 0.00014
Zero quality factor	0.48340 ± 0.00006	0.47822 ± 0.00006
Pole frequency (Hz)	14.4088 ± 0.0007	14.4365 ± 0.0009
Pole quality factor	0.49653 ± 0.00002	0.49592 ± 0.00002
χ^2/ndf	451480./167021	271480./77103

Table 2: ***Models for the sensing of the raw channels*** $Pr\_B1\_\{d2, d3\}\_ACp\_40K$*, valid up to 40 kHz. The delays are given related to the absolute GPS time. Systematic errors are:* $\pm 3\%$ *on the modulus and* ± 30 *mrad on the phase from the fit residuals, and* ± 4 μs *on the delay.*

2.2 Figures

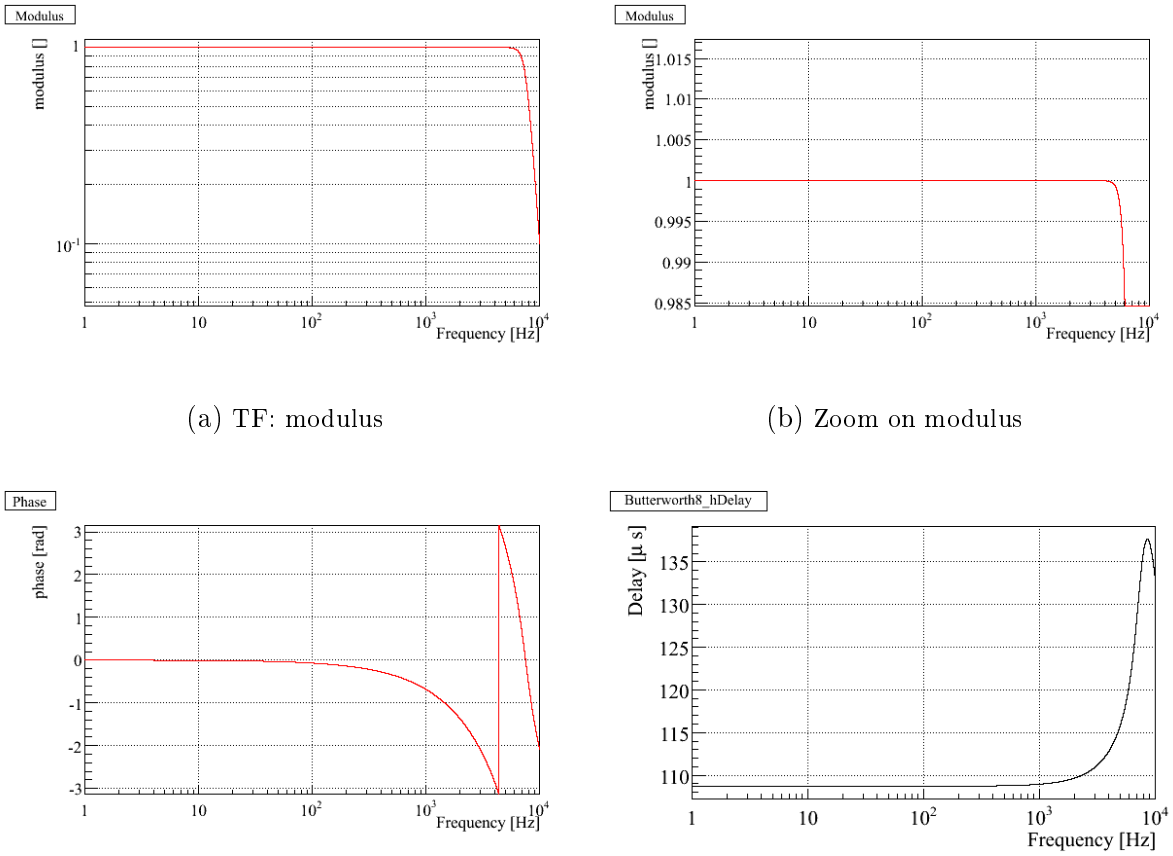

(a) TF: modulus

(b) Zoom on modulus

(c) TF: phase

(d) Equivalent delay

Figure 1: ***Model of the ADC board digital anti-alias filter of the dark fringe channel*** *sampled at 20 kHz: 8th order Butterworth filter with cut-off frequency at* 7503.65 *Hz.*

3 Calibration of the mirror actuation

The mirror actuation is defined as the TF (with modulus in m/V) from the correction signal sample in the Virgo DAQ to the induced mirror motion using the GPS time as reference.

In the plots that are shown, the part from the mechanical model of the pendulum has been removed. The model is defined as a 2nd order low-pass filters with $f_0 = 0.6\,\mathrm{Hz}$ and $Q = 1000$.

The mirror motion used as reference is **the effective motion on the arm differential length.** It means that the induced BS mirror motion perpendicular to its axis is $\sqrt{2}$ lower than what is measured and given in this note.

3.1 Description of the measurements for BS, NE and WE

The detailed description can be found in the note [1].

The first step consists in measuring the mirror actuation in High Power (HP) mode using free swinging Michelson data: the differential arm length ΔL(m) is reconstructed from the data and the transfer function (TF)[1] of ΔL over the injected noise (V) is computed to get the actuation transfer function in m/V (in the following plots, the mechanical response of the pendulum has been removed for better visibility).

Before and during VSR2, about 15 lines have been injected between 6 Hz and 1.5 kHz. Before VSR2, they have been injected with different amplitudes in order to check the linearity of the measurement. During VSR2, they have been injected every two weeks with fixed amplitudes in order to monitor the stability of the actuation response. After VSR2, additionnal lines were injected and up to higher frequency (2.3 kHz) in order to better constrain the parameterization. Different amplitudes were also injected again.

The second step consists in measuring the LN1/HP actuation ratio comparing in both modes the current flowing in the coil as function of the injected noise[2]. Two types of measurements have been done: (i) injection of lines at the same frequencies as the free Michelson line injection and (ii) injection of white noise from a few Hz to a few kHz. The line injections allow to have precise measurements at the frequencies where the actuation is known in HP mode. The white noise injections are used to check the behaviour of the ratio at all frequencies. The noise has been injected with different amplitudes to check the TF linearity.

In December 2009, close to the end of VSR2, the noise amplitude sent to the BS coils has been increased since it was below the signals from the dampers: compared to the previous

[1] The TFs are computed using FFT lenght of 13 s for datasets shorter than 200 s. For longer datasets of d s, the FFT length is $d/10$. Only the points with coherence higher than 80% have been used.

[2] A FFT length of 4 s was used to compute the TFs. Only points with coherence larger than 99% and 99.999% were used for white noise and line injections respectively.

results, the measurements have thus been extended below ~ 30 Hz.

As a final step, the mirror actuation in LN1 mode is computed multiplying the mirror actuation in HP mode by the LN1/HP ratio. The multiplication is done using the data points measured at the free Michelson line frequencies. The data are then fitted by a model including poles and zeros.

As for the actuation in HP mode, the plots of A are not corrected for some delays. Both the "raw delay" (only corrected for the light propagation time) and the corrected delay are given in the tables with the model parameters.

3.2 Actuation calibration of BS, NE and WE

The parameters of the parameterizations fitted on the mirror actuation measurements are given in the table 4 for the configurations used in the longitudinal controls and in the table 5 for the configurations used for the hardware injections.

The figures of the different data and fit are shown in the section 3.5.

3.2.1 Actuation in HP mode

Free swinging Michelson data were analysed to extract the actuation response A in HP mode. Statistical errors are below 1%/10 mrad in modulus and phase respectively for the data points that were measured from June 2009 to January 2010. They are slightly higher for the additionnal points of the post-run measurements.

Time stability and linearity - The results were checked for time variability and for linearity (as function of the noise injected amplitude). The modulus and the phase are compatible with constants within statistics (see for example appendix A.1) and systematic error are thus considered as negligible.

NE mirror actuation using the L-R coils - The analysis of the data in free Michelson for the NE mirror actuation using the L-R coils show strange behaviour at high frequency (around 800-900 Hz). It has been found using other measurements that the NE, coil L, is not well fixed and induces a resonance of the mirror motion (around 800-900 Hz in free Michelson data and around 1100-1200 Hz in step 12 data). See logbook entries 24332, 24353 and 24532 for more details.

3.2.2 LN1 to HP TF ratio

Statistical errors are of the order of 1%/10 mrad in modulus and phase respectively from 5 Hz to a few kHz.

Time stability of the ratio - The measurements during VSR2 (July 3rd 2009 to January 8th 2010) were done with the same configurations every week, in particular the same injected noise. It allows to check the time stability of the LN1 to HP ratio. The ratio as function of time is shown at some frequencies for all the coils (for example, see figure 8). No variations are observed within the statistical error.

When strong amplitudes are injected (lines), the statistical errors are reduced and some variations of the modulus ratio, at the level of 1% to 2%, are observed between the pre- and post-run strong injections.

Linearity of the ratio - During pre- and post-run measurements, different levels of noise injections have been done in order to check the linearity of the actuation response. The modulus and phase as function of the amplitude of the current flowing in the coil in HighPower mode are shown at some frequencies for all the coils (see for example the figure 9).

Variations are lower than 1% in modulus and the phase are compatible with being stable within better than 10 mrad, except for three coils:

- **WE, coil up**: the modulus ratio differs by up to 3% between different injected noise, and the phase difference shows some variations that can be interpreted as an uncertainty below ~ 4 μs(see figure 16(b)).
- **WE, coil right**: same as for coil up (see figure 17(d)).
- **BS, coil down-left**: the modulus ratio decreases by up to 6% when the amplitude of the injected increases by a factor of 20 (see figures 25 and 29(b)). No effect is seen on the phase. Note that this coil has some noise issues in HP mode, coming from the DAC or the coil driver: see logbook entry 25006. It has been checked that the TF measured in HP mode is the one that change when injecting different amplitudes. The TF measured in LN1 mode is stable.

In order to compute the actuation response in LN1 mode, an average of the LN1/HP ratio of the corresponding coils is calculated: the effect of the non-linearities of theses three coils are thus reduced. A systematic error of 3% on the modulus is thought to be conservative.

Note that the current sensing channel $Ca\_BS\_RM\_CoilDR$ of **coil down-right of BS** has been found to be noisy (see logbook entries 24860 and 25006). It provoks less good measuremeents of the LN1/HP ratio for this coil below a few 100's Hz as can be seen in the figure 29(d).

Differences between coils - For a given mirror, the LN1/HP ratio is different for the different coils. This might induce systematic errors since their average is used when computing the WE actuation in LN1 mode from the actuation in HP mode. The differences are of the order of 1% to 2% in modulus: the possible systematic errors that it could induce should be

lower than 1%. The differences concerning the phase looks negligible (lower than 10 mrad at 1 kHz), except between the **Up and Down coils of WE** where the phase difference at 1 kHz is 100 mrad, which is equivalent to 16 μs. It could add a systematic error of $\sim$ 10 μs on the WE actuation using the U-D coils.

Mirror actuation of NE using L-R coils - It has been found that the **coil left of NE** (or magnet) is not well fixed and induces a resonance of the mirror motion. See logbook entries 24332, 24353 and 24532 for more details.

3.2.3 Cross-check of BS mirror actuation in LN1 mode

The standard way to measure the mirror actuation in LN1 mode is done as a combination of measuremnts of the actuation in HP mode and measurement of the LN1/HP ratio. In order to cross-check the results, a direct measurement of the BS mirror actuation in LN1 mode has been performed using free swinging Michelson data. Due to limited dynamic of induced mirror motion in LN1 mode, only some frequencies below 70 Hz have been measured, with poor statistical errors. The result is shown in the figure 35. The measurements agree with the standard ones, within the large statistical errors of the order of 5%/5 mrad in modulus and phase respectively. Hence, no systematic errors can be highlighted.

3.2.4 Comparison between new and previous actuation parameterizations

The new parameterizations (in LN1 mode) have been compared to the one from note VIR-0576A-09 in the figure 36. The previous models were claimed to be valid up to $\sim$ 1.5 kHz with uncertainties of the order of 2%/20 mrad in modulus and phase respectively, while the new ones are measured up to 2 kHz.

For the end mirrors, both models agree within better than 2%/20 mrad below 1 kHz for the modulus and phase respectively. At 2 kHz, the discrepancy increases up to 20%/200 mrad.

For the BS mirror, the modulus agree within better than 1% up to 2 kHz. The phase agree within 10 mrad up to 1 kHz and the discrepancy increases up to 200 mrad at 2 kHz.

The discrepancies between the old and new parameterizations are well within the model residuals, 2%/20 mrad in the domain where both are valid, from 5 Hz to 1 kHz. As shown in the parameterization residuals from the previous parameterizations, the statistical uncertainties between 1 kHz and 1.5 kHz were increasing up to 5%/50 mrad.

3.3 Calibration of the PR mirror actuation

The PR mirror actuation cannot be calibrated using free swinging Michelson data. It is calibrated comparing its response to the BS mirror actuation in HP mode.

The PR-WI cavity is locked. The BS mirror is used as a folding mirror. A motion of PR, BS or WI has the effect of changing the cavity length. This can be seen by the photodiode at the ITF output port (channel Pr_B1p_ACp) which is used for the locking of the cavity. The correction signals are sent to the PR mirror actuation. The BS suspension is set in HP mode.

Adding the same signal to the corrections sent to BS or PR has the same effect in terms of changing the cavity length (i.e. the optical response), provided a factor $\sqrt{2}$ is taken into account because of the 45° orientation of the BS mirror (this factor is already included in the gain measured on the BS mirror actuation).

The closed-loop TF of the locked cavity is measured into two consecutive datasets: one with noise injected to the PR mirror actuation and one with noise injected to the BS mirror actuation. The TFs of the injected noise (i.e. Ca_PR_zMir) to the ITF output power (Pr_B1p_ACp) are two measurements of the closed-loop TF of the locked cavity. They can be written as function of the power sensing S, the optical response O of the cavity and the mirror actuation response (i.e. $P_{PR}A^{HP}_{PR}$ for the PR mirror):

$$TF\left[\frac{Pr\_B1p\_ACp}{Ca\_PR\_zMir}\right] = \frac{SOP_{PR}A^{HP}_{PR}}{1-G_{olg}} \quad (1)$$

$$TF\left[\frac{Pr\_B1p\_ACp}{Ca\_BS\_zMir}\right] = \frac{SOP_{BS}A^{HP}_{BS}}{1-G_{olg}} \quad (2)$$

with the open-loop gain $G_{olg} = SOP_{PR}A_{PR}F_{PR}$ (F_{PR} is the filter between the output power and the correction signal sent to the PR mirror). The sensing response S and the optical response O are the same for all the mirrors. The pendulum mechanical response models P_i are also the same. The ratio of both TFs thus gives a measurement of A^{HP}_{PR}/A^{HP}_{BS}.

The ratio has been measured after VSR2 between 1 Hz and 300 Hz with errors of the order of 5-10% (see figure 37, and multiplied by the measured actuation TF of the BS mirror (using the measured points). The measured response of the PR mirror actuation is given in the figure 38. The fit has been performed between 1 Hz and 300 Hz. In order to have a response above 300 Hz compatible with the arm mirror actuation, the pole and the zero above 100 Hz have been fixed to the values from the WE mirror actuation through the U-D coils in HP mode. The gain, delay, a pole and a zero were let free. The result is given in the table 6.
The parameterization describes the data within 5% in modulus and 50 mrad in phase below 300 Hz. Systematic errors from the BS actuation in HP mode being negligible, no additionnal errors are set to the PR parameterization.

Below 300 Hz, the shape of the PR mirror actuation is closer to the arm mirror actuation TFs than to the BS one. This is expected since the PR reference mass is made of stainless steel as the arm ones. The frequency dependence due to the Eddy currents should thus be similar.

3.4 Tables

Parameter	Values	Names of real pulsations
7 zeros (rad/s)	-268.962	z_1
	$-\mathrm{j} \times 53346.9$ and $+\mathrm{j} \times 53346.9$	z_2
	$-\mathrm{j} \times 65336.3$ and $+\mathrm{j} \times 65336.3$	z_3
	$-\mathrm{j} \times 117520$ and $+\mathrm{j} \times 117250$	z_4
8 poles (rad/s)	-31423.2	p_1
	$-21492 - \mathrm{j} \times 10099.1$ and $-21492 + \mathrm{j} \times 10099.1$	p_2, p_3
	$-13768 - \mathrm{j} \times 19533.1$ and $-13768 + \mathrm{j} \times 19533.1$	p_4, p_5
	$-4416.78 - \mathrm{j} \times 22931.4$ and $-4416.78 + \mathrm{j} \times 22931.4$	p_6, p_7
	-266.764	p_8

Table 3: ***Model of the 8th order anti-alias filter of the DAC between the DSP and the coil driver****. The full expression of the associated TF is given in appendix B.6.*

		WE, U-D coils	NE, U-D coils	BS, four coils
HP	Gain (μm/V)	12.765 ± 0.006	13.46 ± 0.01	89.24 ± 0.01
	Raw delay (μs)	(598.4 ± 0.6)	(610.3 ± 0.5)	(622.7 ± 0.03)
	Φ_0 (rad)	0	0	π
	Pole frequency (Hz)	53.40 ± 3.7	53.9 ± 5.4	42.20 ± 0.37
	Zero frequency (Hz)	57.67 ± 4.5	59.2 ± 6.6	42.96 ± 0.38
	Pole frequency (Hz)	190.1 ± 12	194.8 ± 17	–
	Zero frequency (Hz)	226.4 ± 14	232.2 ± 28	–
	Pendulum	One 2nd order low-pass filter: $f_0 = 0.6$ Hz, $Q = 1000$		
	χ^2/ndf	67.4/92	83.2/92	8101.3/84
LN1	Gain (μm/V)	13.334 ± 0.015	13.70 ± 0.021	88.519 ± 0.004
	Raw delay (μs)	(420.6 ± 0.7)	(421.4 ± 0.8)	(380.1 ± 0.2)
	Delay (μs)	271.3 ± 0.7	272.4 ± 0.8	230.8 ± 0.2
	Φ_0 (rad)	0	0	π
	Pole frequency (Hz)	70.72 ± 5.2	79.59 ± 7.7	3506.66 ± 9
	Zero frequency (Hz)	78.77 ± 6.6	90.94 ± 10.2	–
	Pole frequency (Hz)	292.03 ± 29	356.77 ± 47	–
	Zero frequency (Hz)	349.24 ± 32	424.83 ± 51	–
	DAC anti-alias filter	See model in table 3		
	Pendulum	One 2nd order low-pass filter: $f_0 = 0.6$ Hz, $Q = 1000$		
	χ^2/ndf	48.0/88	53.9/90	1860.7/83

Table 4: ***WE (U-D coils), NE (U-D coils) and BS (four coils) mirror actuation parameterizations****, in HP mode and LN1 mode. The models are valid up to 2 kHz. The* χ^2/ndf *of the fits are given. The raw delay is the measured delay that includes the delay from the injection path to the DSP and the delay from the* Pr_B1p *channels sensing. The corrected delay takes as reference the correction channel in the DSP (i.e.* Sc_WE_zCorr*) and does not contain the B1 sensing delay nor the delay for the injection part (raw delay with 100* μs *less for the PrCa to DSP delay and* 49.3 μs *less from the dark fringe sensing:* $delay = raw\_delay - 100 - 49.3$ μs*). Applying these TFs to zCorr should enable to estimate the induced motion at absolute GPS time.*

		WE, L-R coils	NE, L-R coils
HP	Gain (μm/V)	12.964 ± 0.008	12.715 ± 0.010
	Raw delay (μs)	(593.4 ± 0.6)	(638.8 ± 3.5)
	Φ_0 (rad)	0	0
	Pole frequency (Hz)	60.4 ± 5.1	63.68 ± 3.4
	Zero frequency (Hz)	65.4 ± 6.3	70.76 ± 4.0
	Pole frequency (Hz)	206.7 ± 17	165.1 ± 19
	Zero frequency (Hz)	242.5 ± 18	179.3 ± 22
	Pendulum	One 2nd order low-pass filter: $f_0 = 0.6\,\mathrm{Hz}$, $Q = 1000$	
	χ^2/ndf	110.2/92	9.6/48
LN1	Gain (μm/V)	13.26 ± 0.029	13.95 ± 0.079
	Raw delay (μs)	(421.4 ± 1.0)	(459.9 ± 3.5)
	Delay (μs)	472.1 ± 1.0	510.6 ± 3.5
	Φ_0 (rad)	0	0
	Pole frequency (Hz)	72.37 ± 6.7	33.0 ± 25
	Zero frequency (Hz)	81.58 ± 8.4	34.4 ± 27
	Pole frequency (Hz)	344.6 ± 40	115.3 ± 28
	Zero frequency (Hz)	413.5 ± 45	133.7 ± 29
	DAC anti-alias filter	See model in table 3	
	Pendulum	One 2nd order low-pass filter: $f_0 = 0.6\,\mathrm{Hz}$, $Q = 1000$	
	χ^2/ndf	51.3/88	7.6/46

Table 5: ***WE (L-R coils), NE (L-R coils) mirror actuation parameterizations****, in HP mode and LN1 mode. The WE actuations model is valid up to 2 kHz. The NE actuations in HP and in LN1 mode have been fitted from 5 Hz to 400 Hz only. The* χ^2/ndf *of the fits are given. The raw delay is the measured delay that includes the delay from the injection path (from PrCa) to the DSP and the delay from the* Pr_B1p *channels sensing. The corrected delay takes as reference the channels sent by the CaInjectors (i.e.* Ca_WE_zMirLR*) and does not contain the B1 sensing delay (raw delay with 100* μs *more since the hardware injections are done from the CaInjectors and* 49.3 μs *less from the dark fringe sensing:* $delay = raw\_delay + 100 - 49.3$ μs*). Applying these TFs to* Ca_WE_zMirLR *channels should enable to estimate the induced motion at absolute GPS time.*

	PR, four coils
Gain (μm/V)	14.66 ± 0.21
Raw delay (μs)	(593.7 ± 14)
Delay (μs)	444.4 ± 14
Φ_0 (rad)	π
Pole frequency (Hz)	21.85 ± 4.0
Zero frequency (Hz)	25.18 ± 4.5
Pole frequency (Hz)	190.1
Zero frequency (Hz)	226.4
Pendulum	One 2nd order low-pass filter: $f_0 = 0.6\,\mathrm{Hz}$, $Q = 1000$
χ^2/ndf	19./42

Table 6: ***PR (four coils) mirror actuation parameterization*** *in its single mode. The PR actuations model is valid up to 300 Hz. The PR actuation has been fitted from 1 Hz to 300 Hz, forcing the pole and zero larger than 100 Hz to the values from the WE mirror actuation in HP mode. The* χ^2/ndf *of the fit is given. The raw delay is the measured delay that includes the delay from the injection path (from PrCa) to the DSP and the delay from the* Pr_B1p *channels sensing. The corrected delay takes as reference the correction channel in the DSP (i.e.* Sc_WE_zCorr*) and does not contain the B1 sensing delay nor the delay for the injection part (raw delay with 100* μs *less for the PrCa to DSP delay and* 49.3 μs *less from the dark fringe sensing:* $delay = raw\_delay - 100 - 49.3$ μs*). Applying these TFs to zCorr should enable to estimate the induced mirror motion at absolute GPS time.*

3.5 Figures

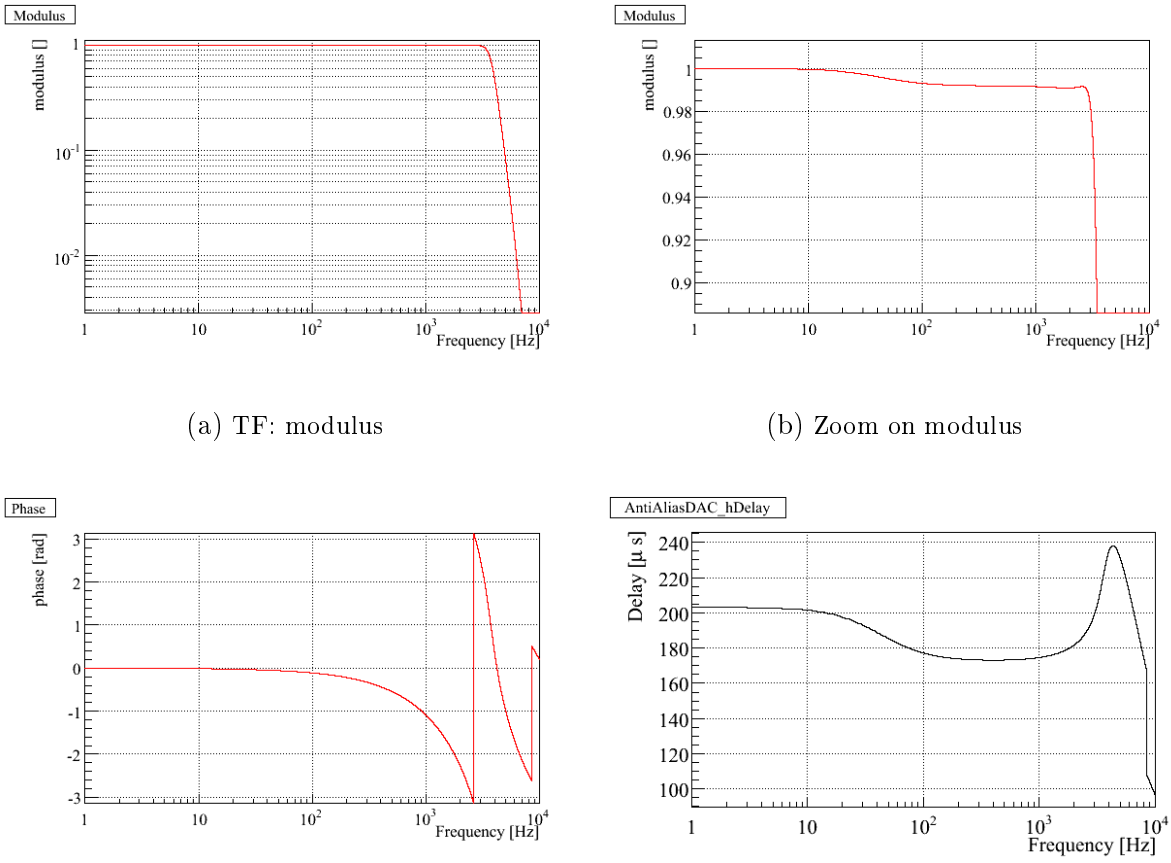

(a) TF: modulus

(b) Zoom on modulus

(c) TF: phase

(d) Equivalent delay

Figure 2: ***Model of the anti-imaging filter of the DAC.***

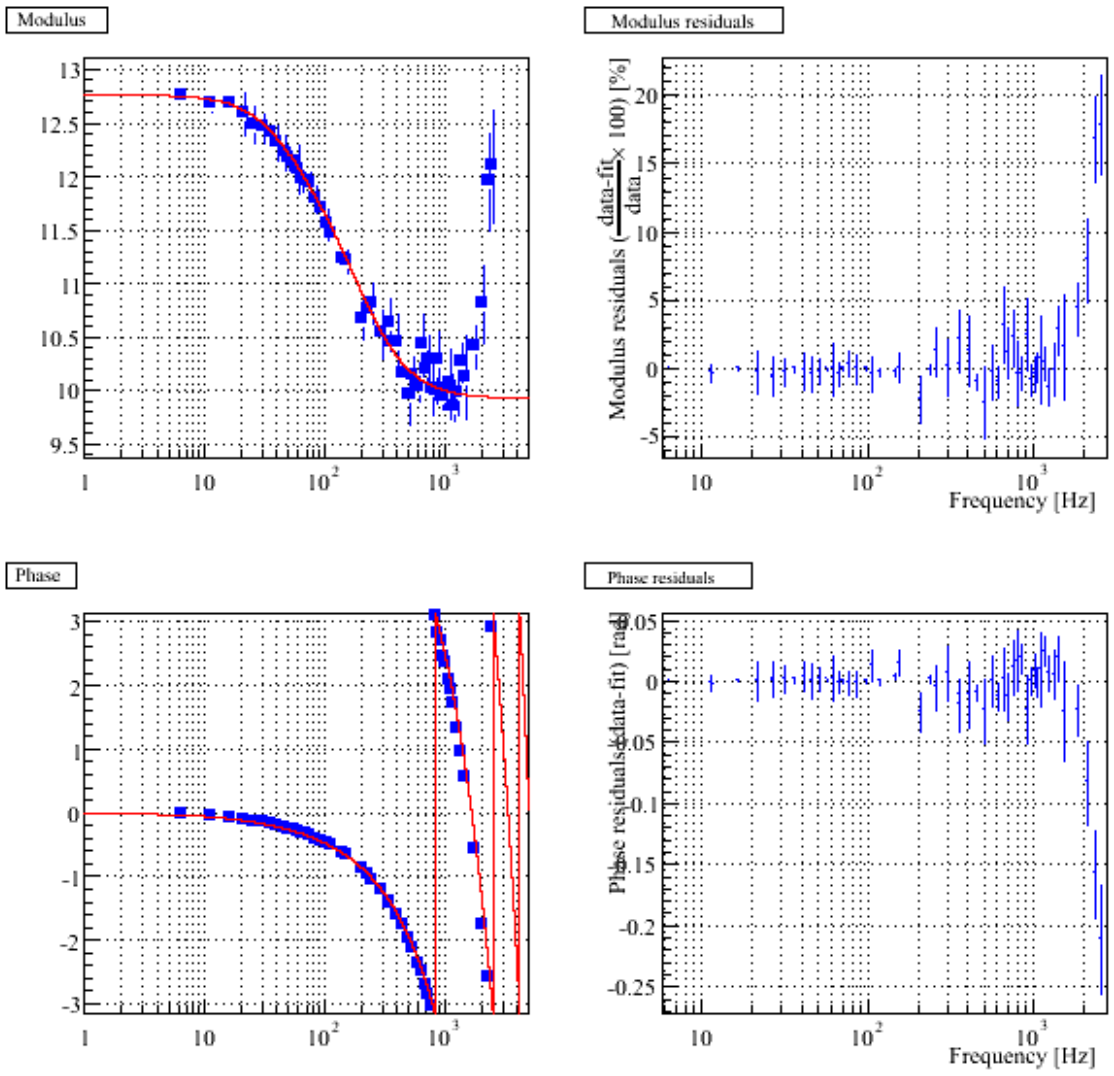

Figure 3: ***Measured actuation of the WE mirror using the U-D coils in HP mode****, fitted model and residuals.*

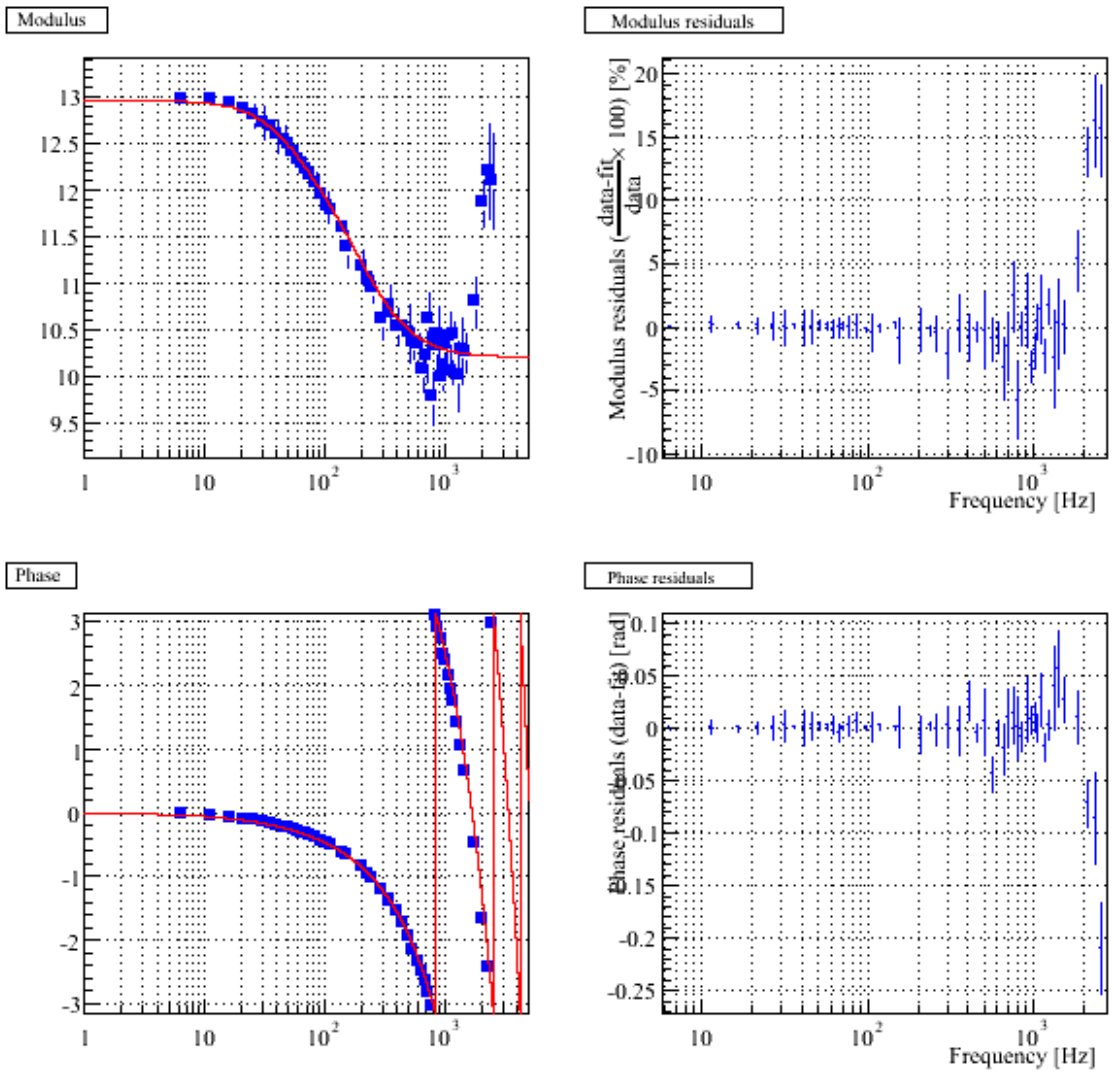

Figure 4: ***Measured actuation of the WE mirror using the L-R coils in HP mode****, fitted model and residuals.*

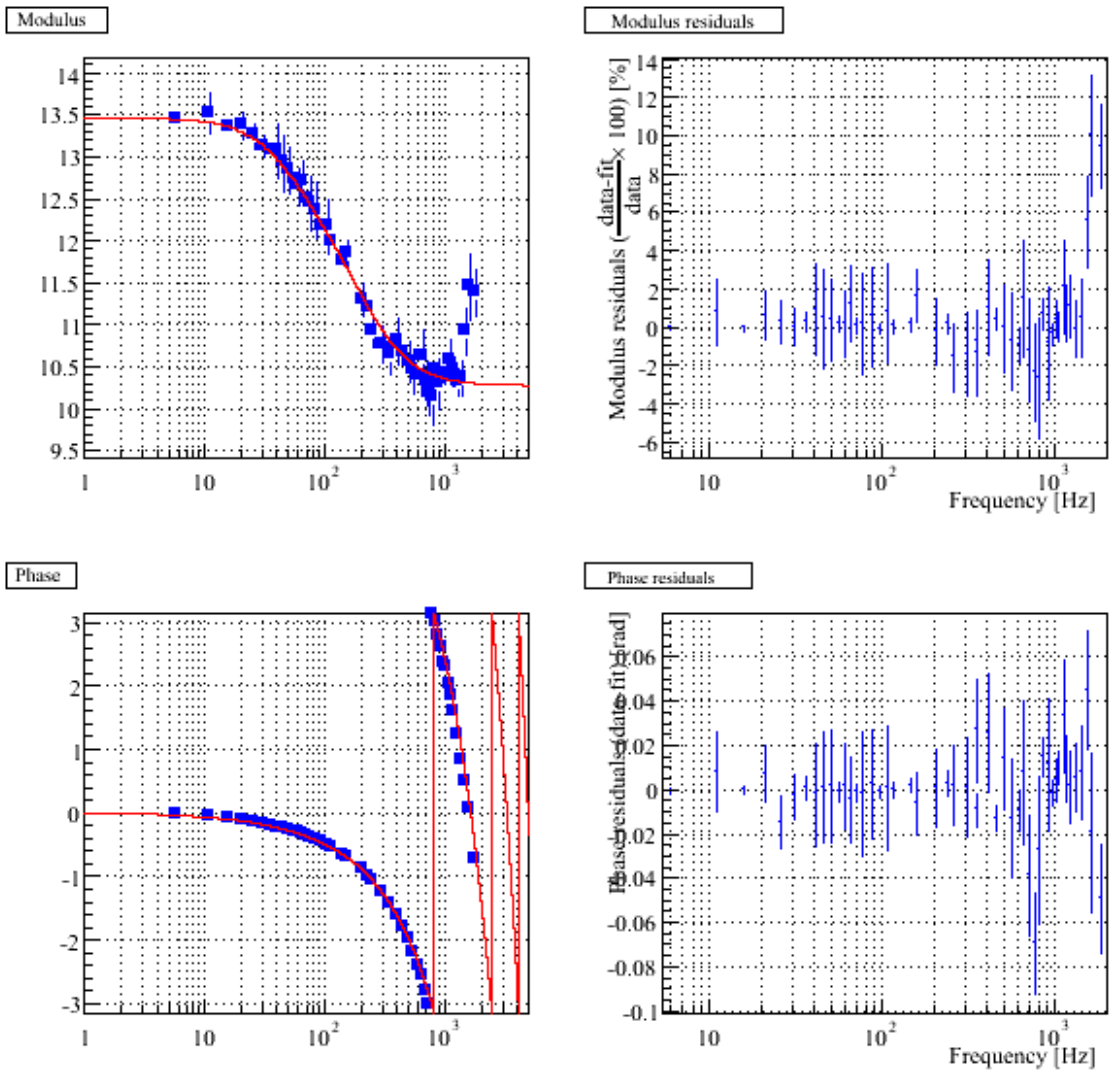

Figure 5: ***Measured actuation of the NE mirror using the U-D coils in HP mode****, fitted model and residuals.*

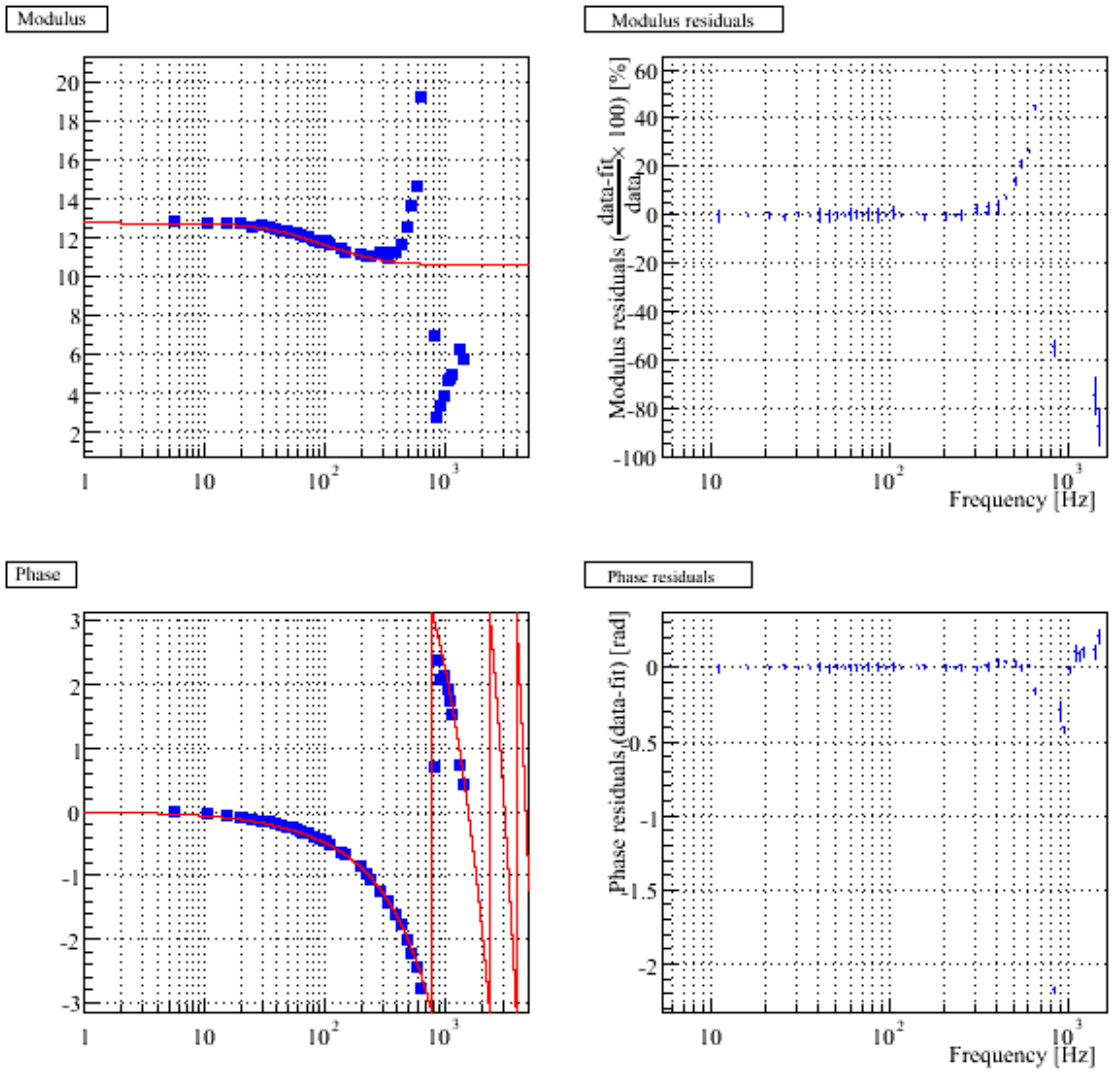

Figure 6: ***Measured actuation of the NE mirror using the L-R coils in HP mode****, fitted model and residuals. The data have been fitted up to 400 Hz only.*

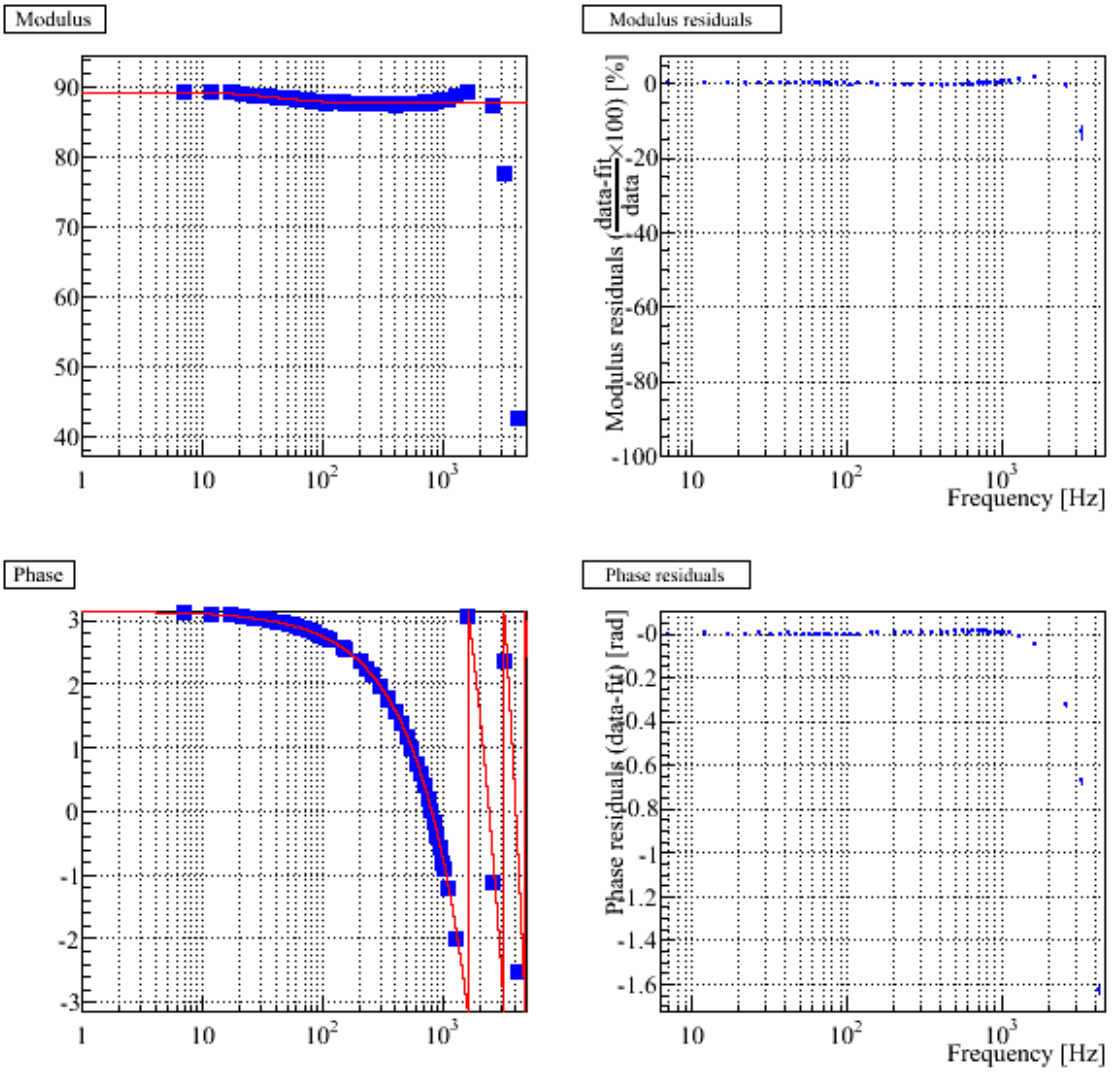

Figure 7: ***Measured actuation of the BS mirror using the four coils in HP mode****, fitted model and residuals.*

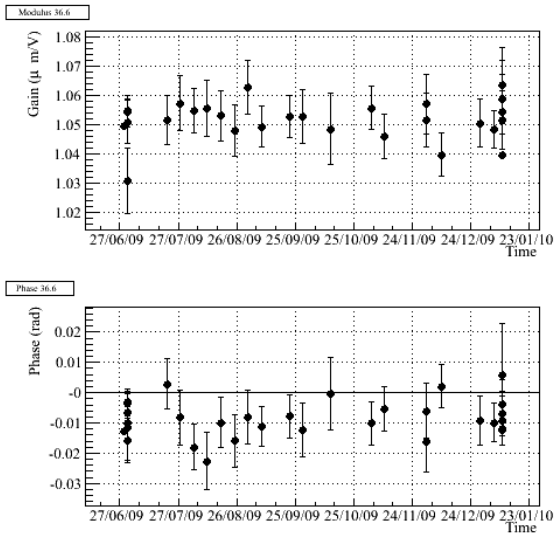

(a) 36.5 Hz

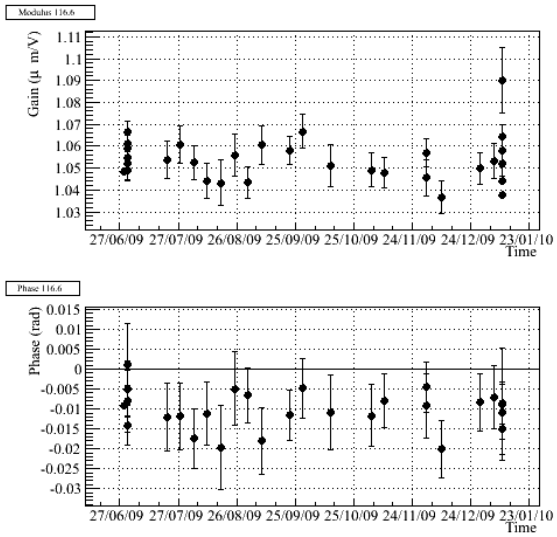

(b) 116.5 Hz

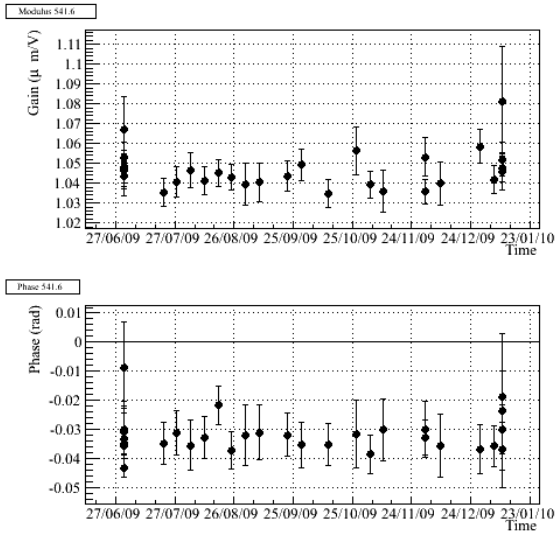

(c) 451.5 Hz

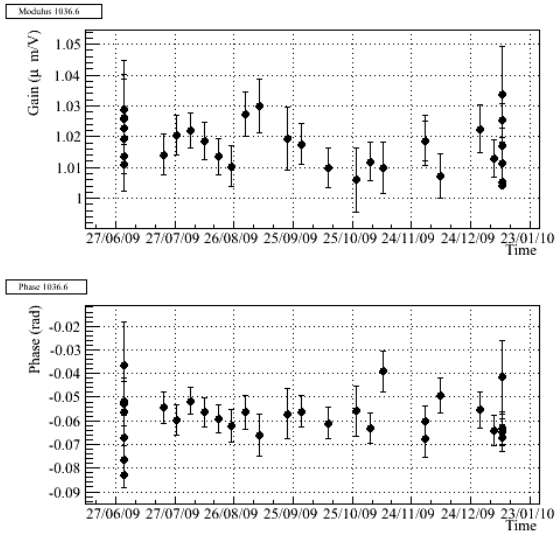

(d) 1036.5 Hz

Figure 8: ***Evolution as function of time (June to September 2009) of the measured actuation TF ratio (LN1/HP) for the up coil of the WE mirror*** *at four different frequencies.*

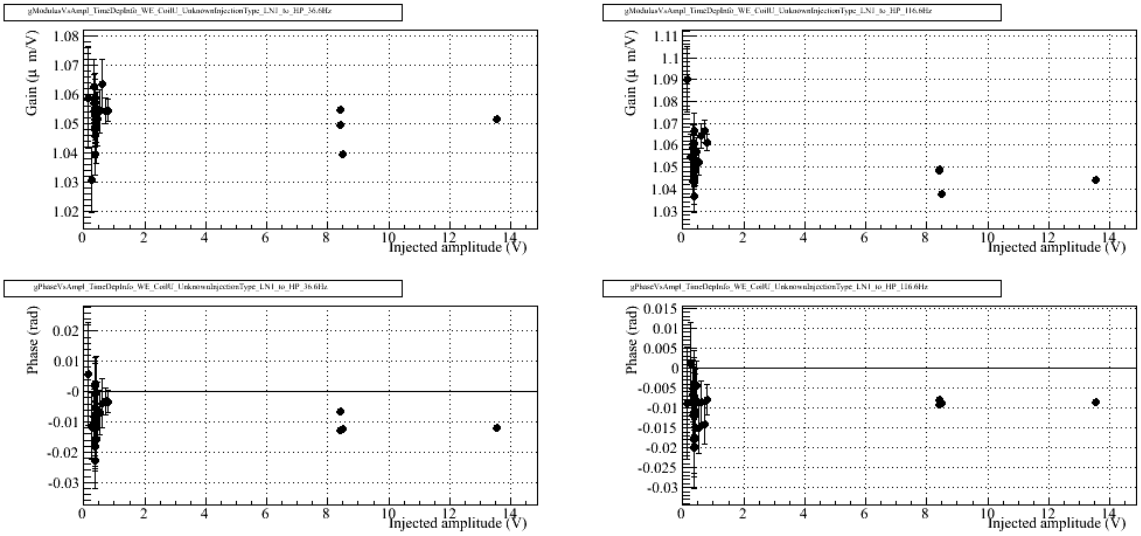

(a) 36.5 Hz

(b) 116.5 Hz

(c) 451.5 Hz

(d) 1036.5 Hz

Figure 9: ***Evolution as function of the signal amplitude of the measured actuation TF ratio (LN1/HP) for the up coil of the WE mirror*** *at four different frequencies. The amplitude in the x-axis is the amplitude of* $V1 : Ca\_WE\_RM\_CoilU$ *during the injections in HighPower mode.*

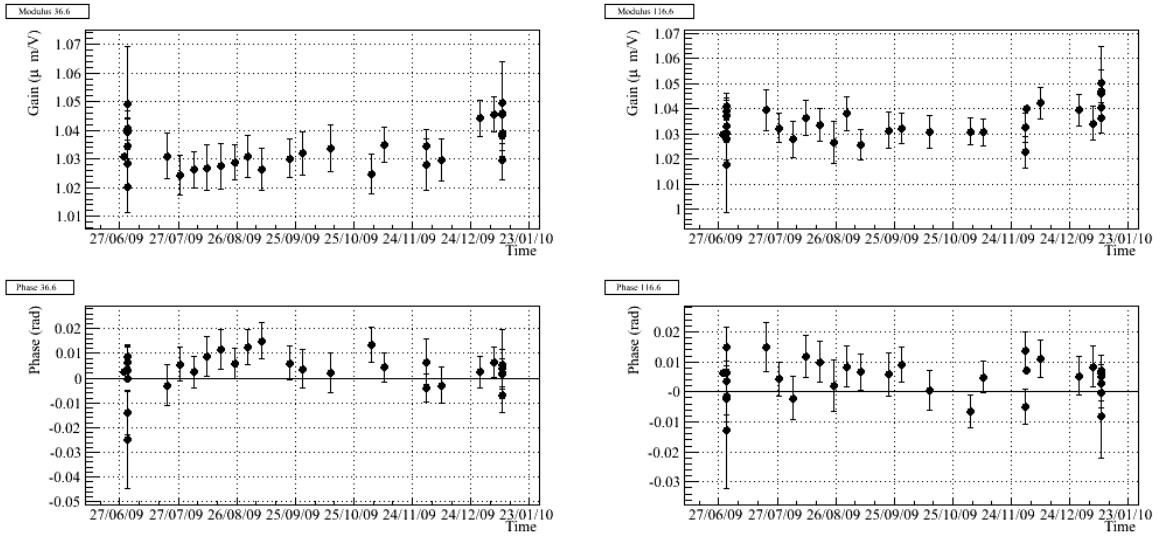

(a) 36.5 Hz

(b) 116.5 Hz

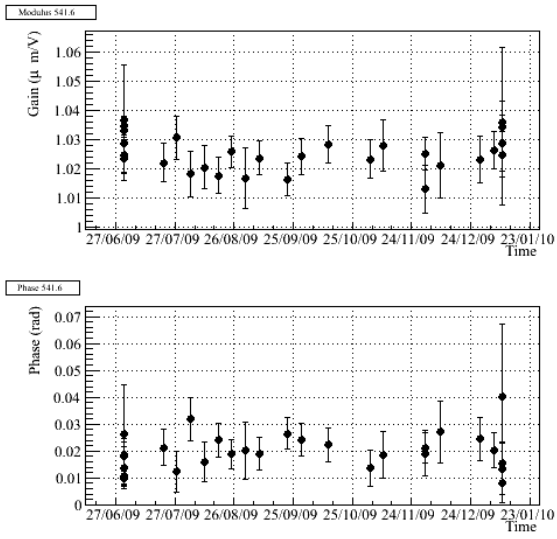

(c) 451.5 Hz

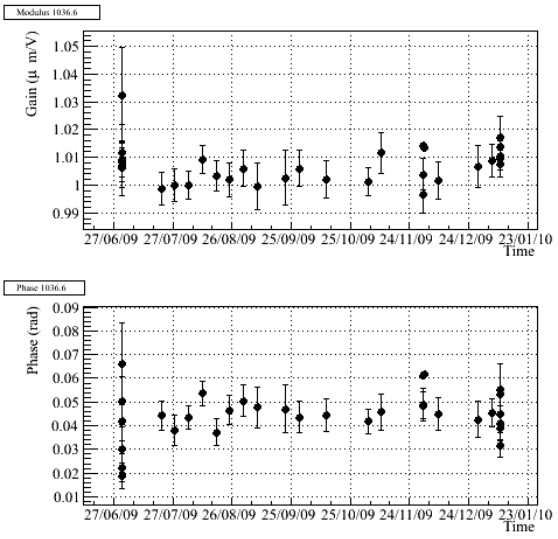

(d) 1036.5 Hz

Figure 10: ***Evolution as function of time (June to September 2009) of the measured actuation TF ratio (LN1/HP) for the down coil of the WE mirror*** *at four different frequencies.*

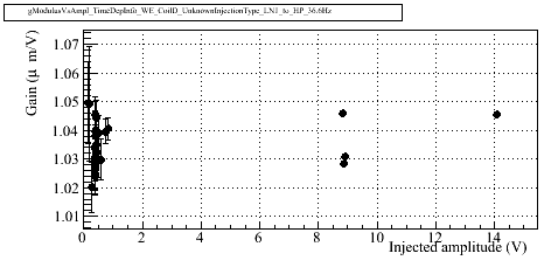

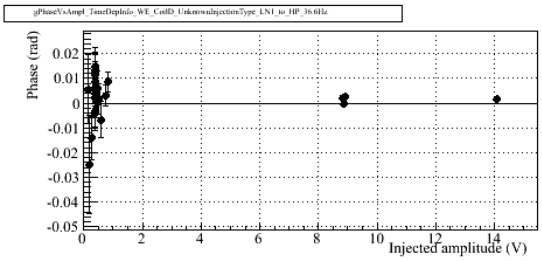

(a) 36.5 Hz

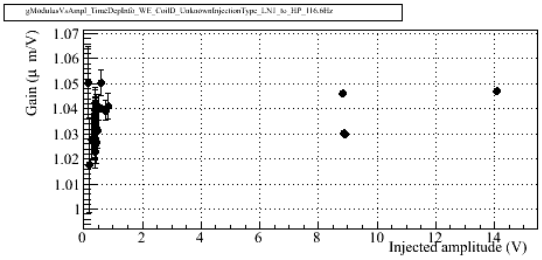

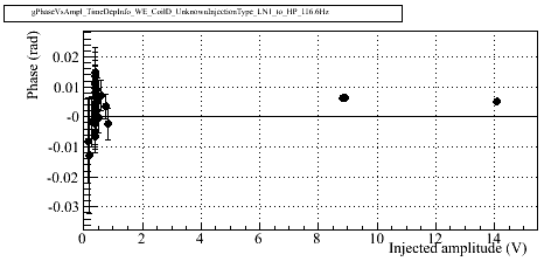

(b) 116.5 Hz

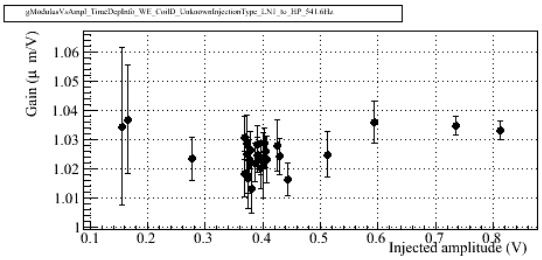

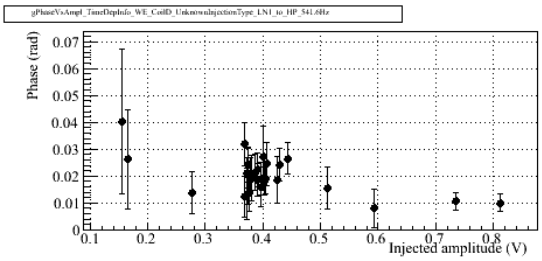

(c) 451.5 Hz

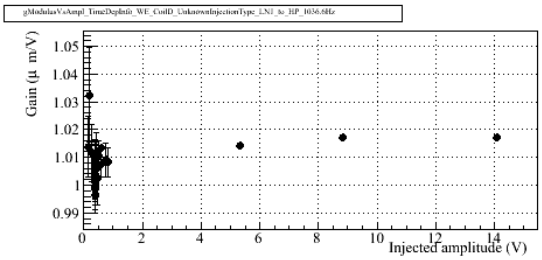

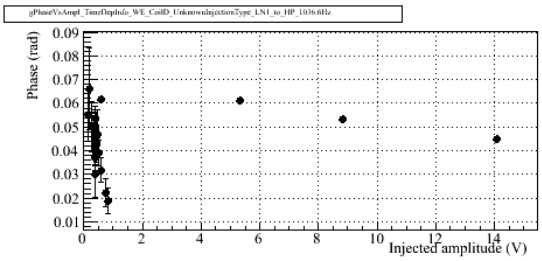

(d) 1036.5 Hz

Figure 11: ***Evolution as function of the signal amplitude of the measured actuation TF ratio (LN1/HP) for the down coil of the WE mirror*** *at four different frequencies. The amplitude in the x-axis is the amplitude of* $V1 : Ca\_WE\_RM\_CoilD$ *during the injections in HighPower mode.*

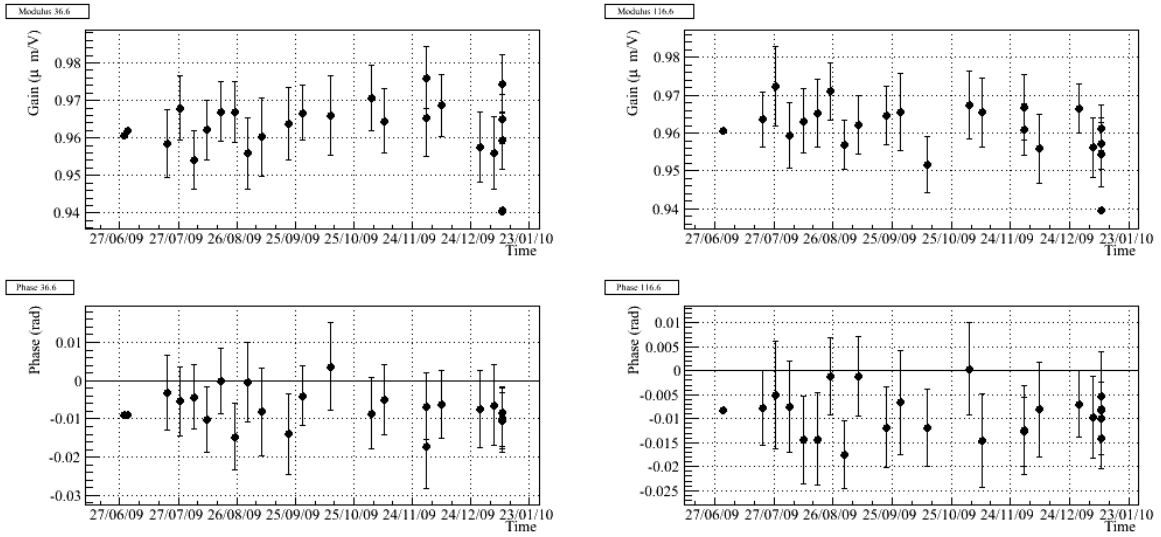

(a) 36.5 Hz

(b) 116.5 Hz

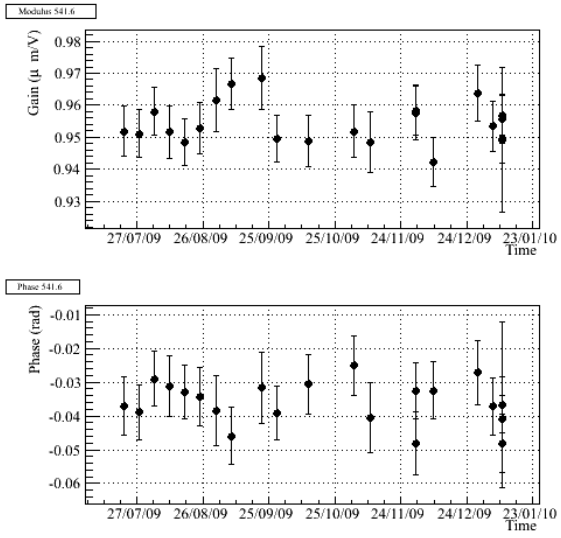

(c) 451.5 Hz

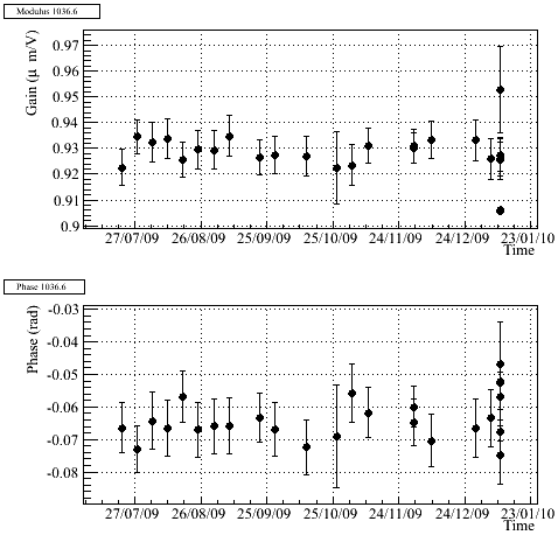

(d) 1036.5 Hz

Figure 12: ***Evolution as function of time (June to September 2009) of the measured actuation TF ratio (LN1/HP) for the left coil of the WE mirror*** *at four different frequencies.*

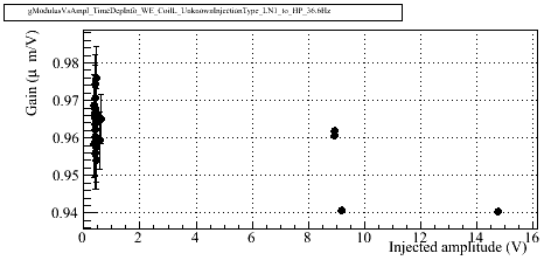

(a) 36.5 Hz

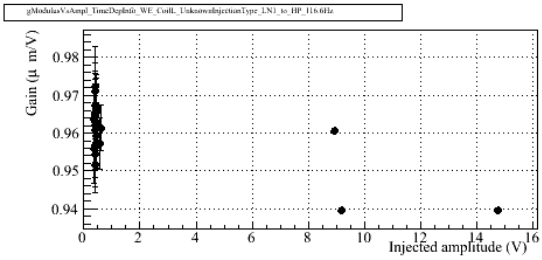

(b) 116.5 Hz

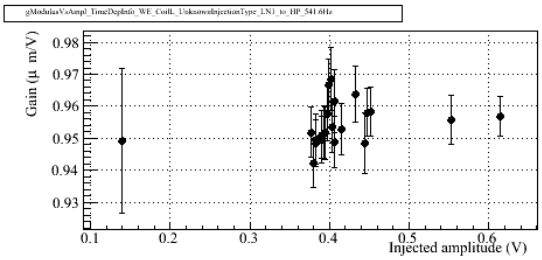

(c) 451.5 Hz

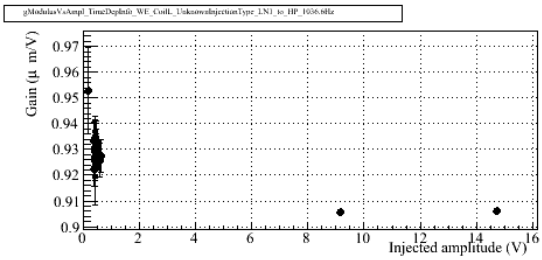

(d) 1036.5 Hz

Figure 13: ***Evolution as function of the signal amplitude of the measured actuation TF ratio (LN1/HP) for the laft coil of the WE mirror*** *at four different frequencies. The amplitude in the x-axis is the amplitude of* $V1 : Ca\_WE\_RM\_CoilL$ *during the injections in HighPower mode.*

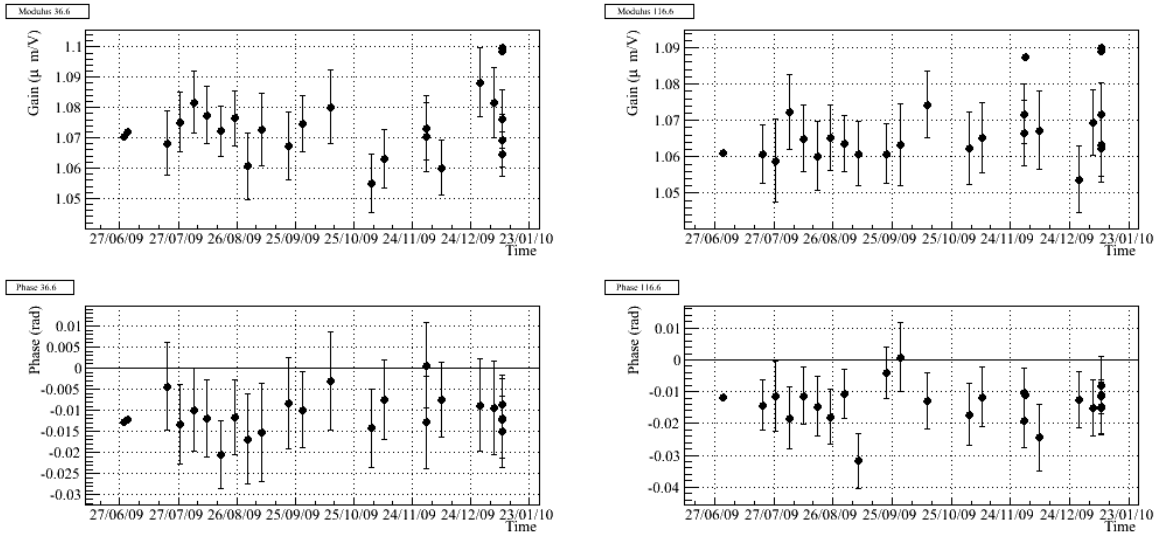

(a) 36.5 Hz

(b) 116.5 Hz

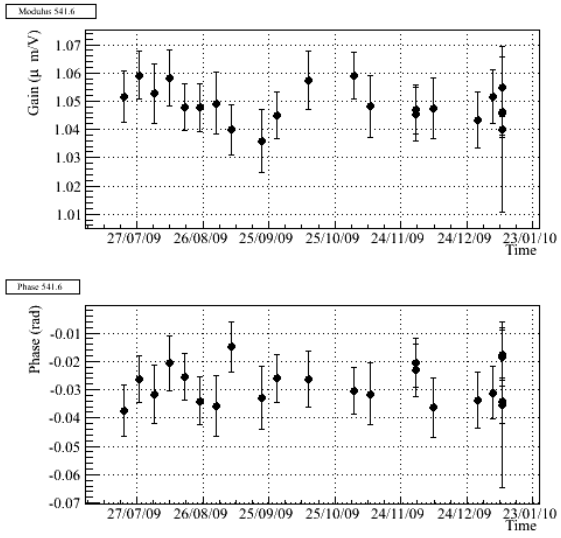

(c) 451.5 Hz

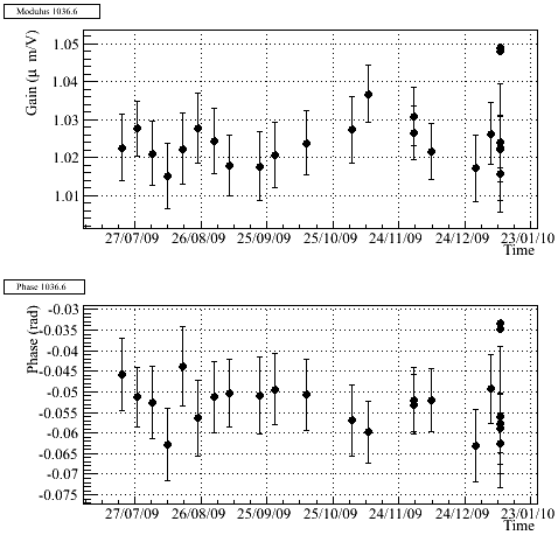

(d) 1036.5 Hz

Figure 14: ***Evolution as function of time (June to September 2009) of the measured actuation TF ratio (LN1/HP) for the right coil of the WE mirror*** *at four different frequencies.*

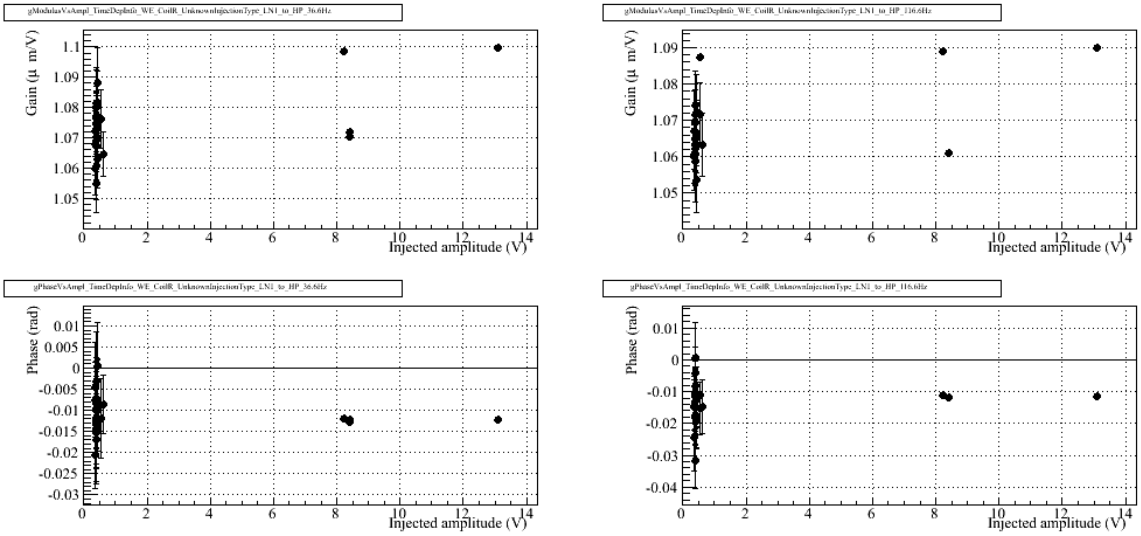

(a) 36.5 Hz

(b) 116.5 Hz

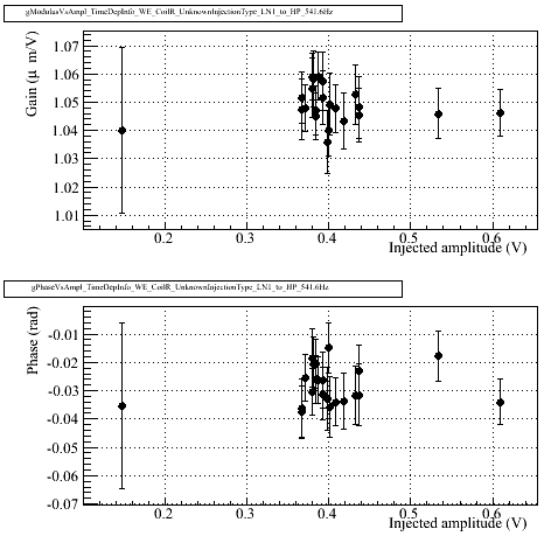

(c) 451.5 Hz

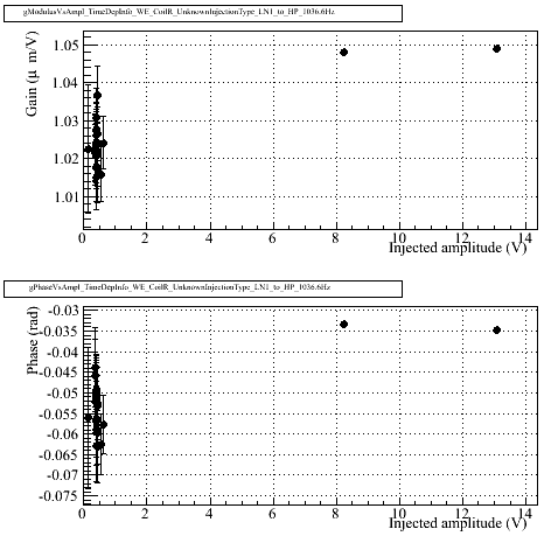

(d) 1036.5 Hz

Figure 15: ***Evolution as function of the signal amplitude of the measured actuation TF ratio (LN1/HP) for the right coil of the WE mirror*** *at four different frequencies. The amplitude in the x-axis is the amplitude of* $V1 : Ca\_WE\_RM\_CoilR$ *during the injections in HighPower mode.*

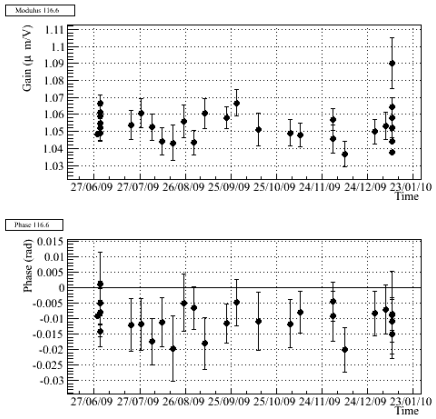

(a) Coil Up, 116.5 Hz.

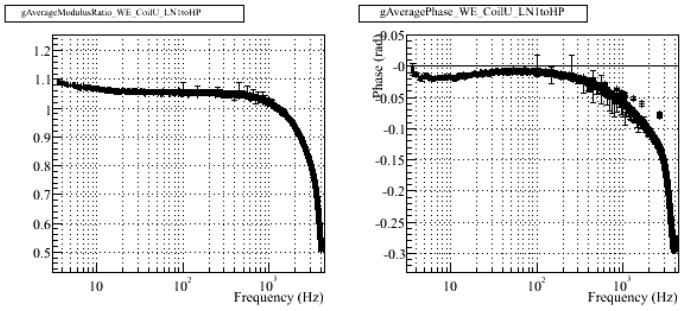

(b) Coil Up, averaged

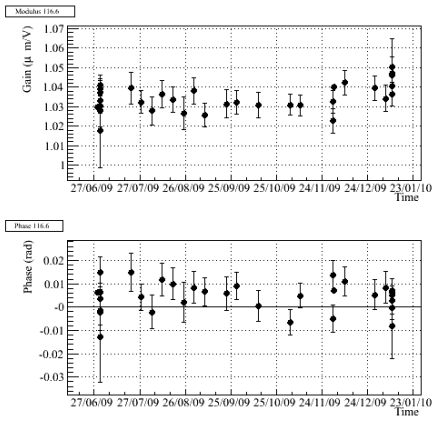

(c) Coil Down, 116.5 Hz

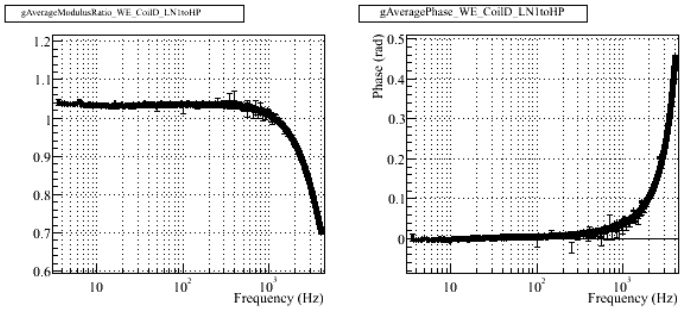

(d) Coil Down, averaged

Figure 16: ***Measured actuation TF ratio (LN1/HP) for the up and down coils of the WE mirror.***

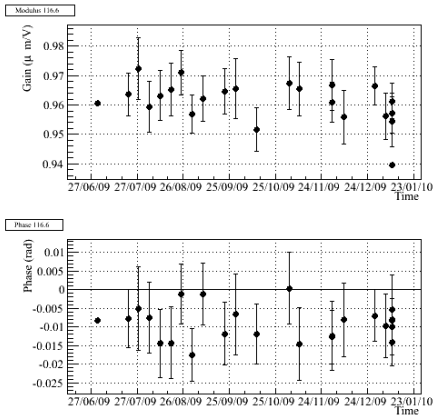

(a) Coil Left, 116.5 Hz

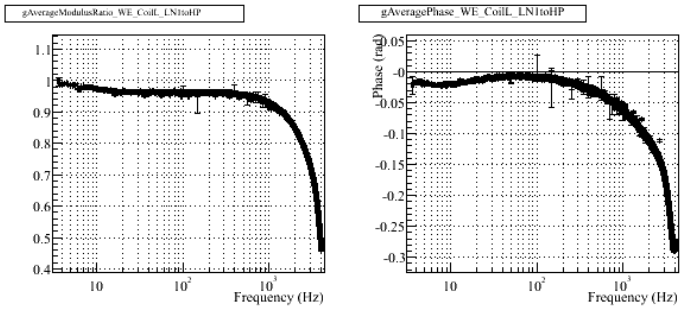

(b) Coil Left, averaged

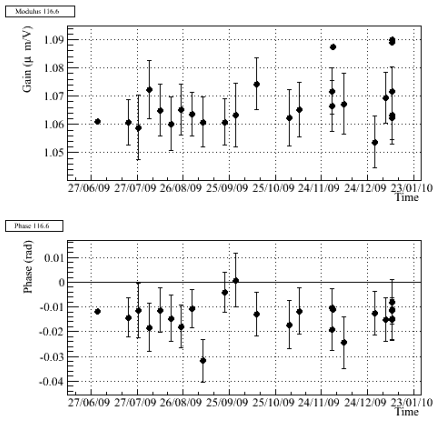

(c) Coil Right, 116.5 Hz

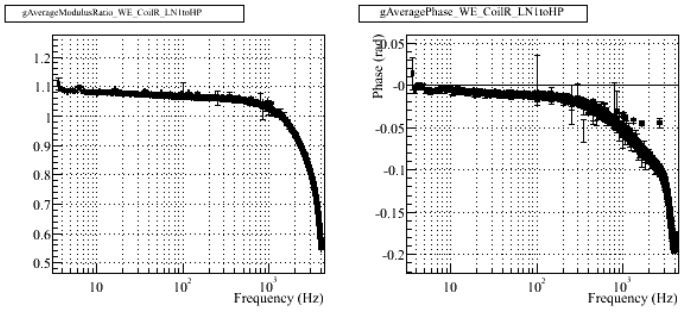

(d) Coil Right, averaged

Figure 17: ***Measured actuation TF ratio (LN1/HP) for the left and right coils of the WE mirror.***

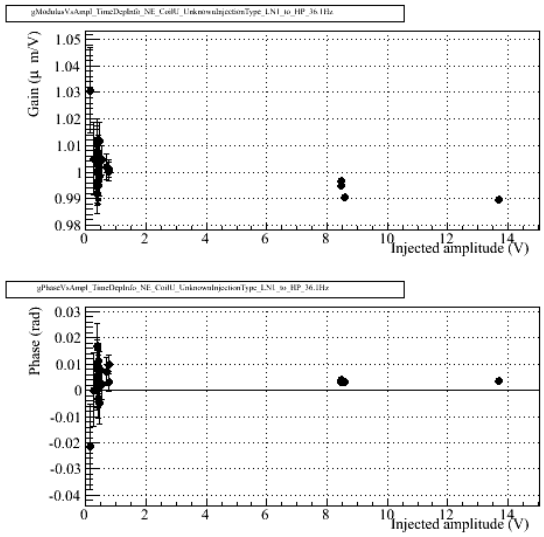

(a) 36.5 Hz

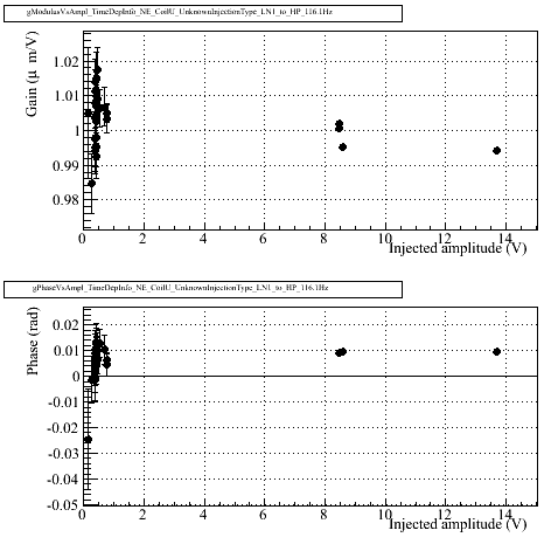

(b) 116.5 Hz

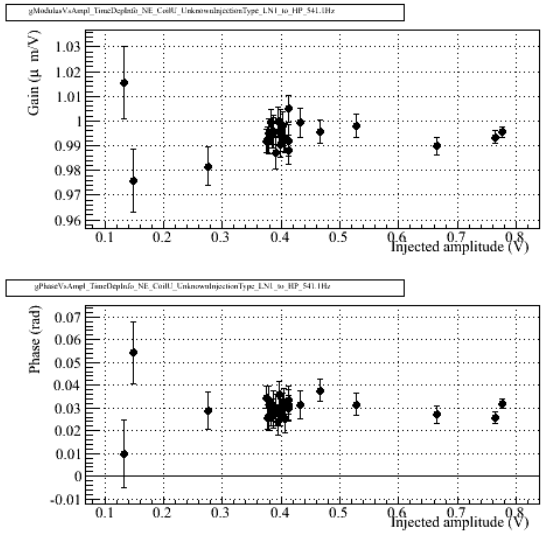

(c) 451.5 Hz

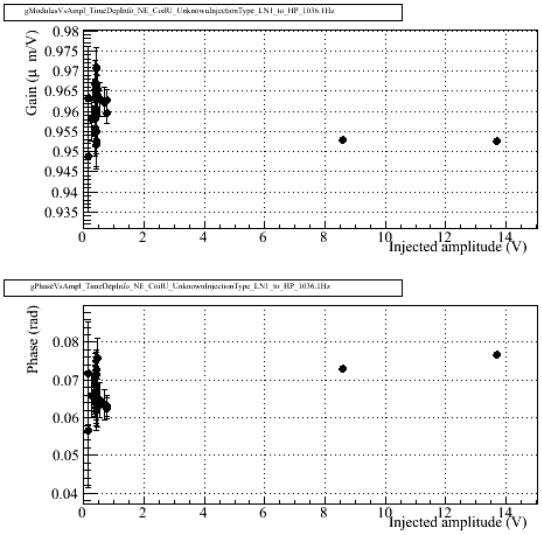

(d) 1036.5 Hz

Figure 18: ***Evolution as function of the signal amplitude of the measured actuation TF ratio (LN1/HP) for the up coil of the NE mirror*** *at four different frequencies. The amplitude in the x-axis is the amplitude of* $V1 : Ca\_NE\_RM\_CoilU$ *during the injections in HighPower mode.*

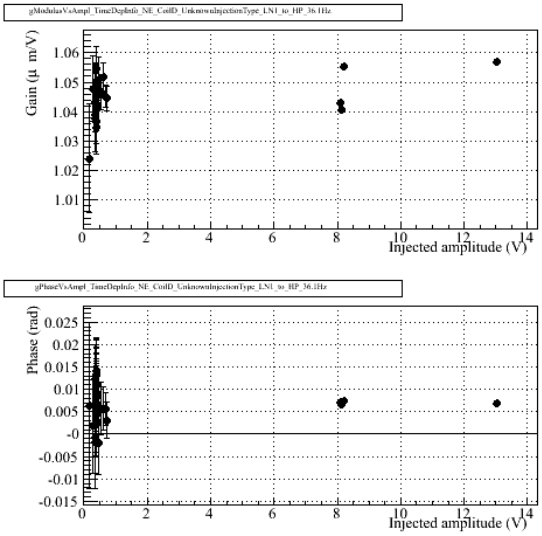

(a) 36.5 Hz

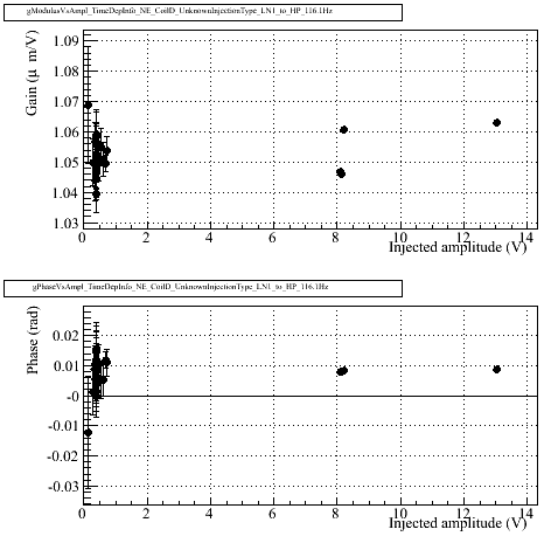

(b) 116.5 Hz

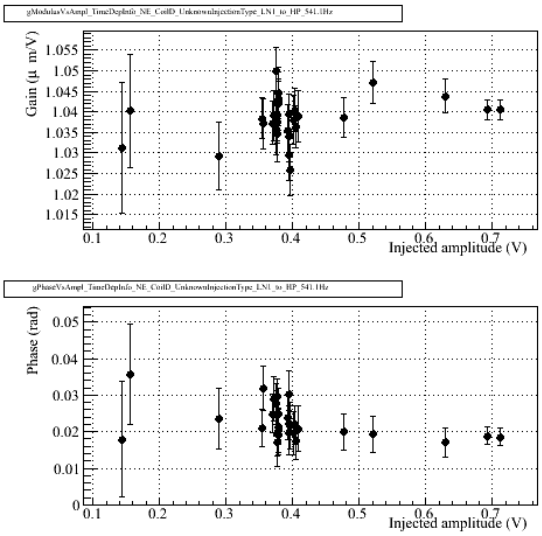

(c) 451.5 Hz

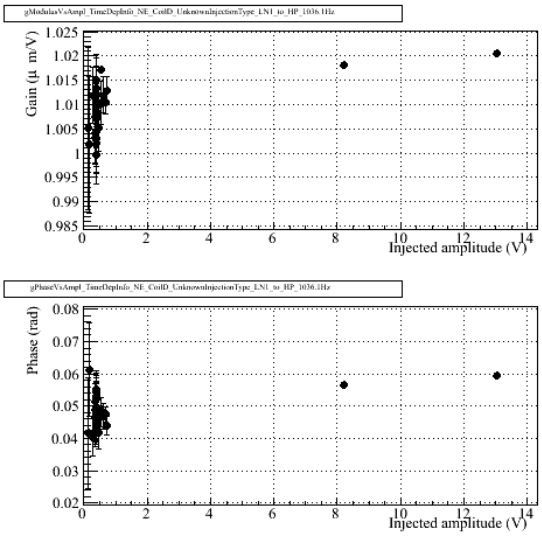

(d) 1036.5 Hz

Figure 19: ***Evolution as function of the signal amplitude of the measured actuation TF ratio (LN1/HP) for the down coil of the NE mirror*** *at four different frequencies. The amplitude in the x-axis is the amplitude of* $V1 : Ca\_NE\_RM\_CoilD$ *during the injections in HighPower mode.*

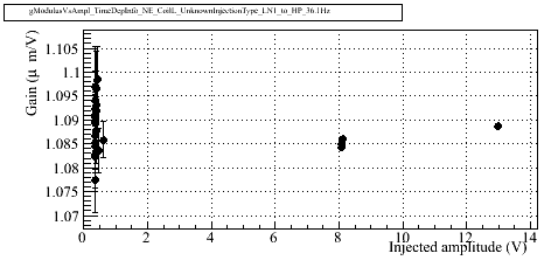

(a) 36.5 Hz

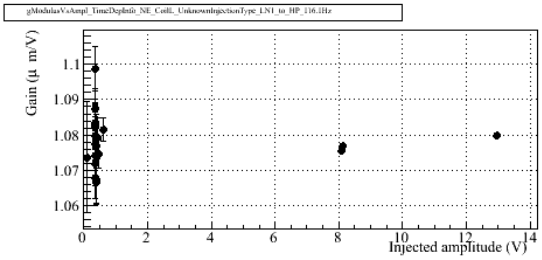

(b) 116.5 Hz

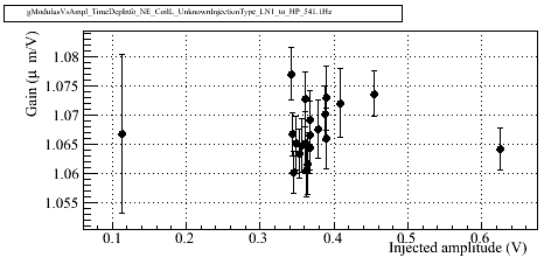

(c) 451.5 Hz

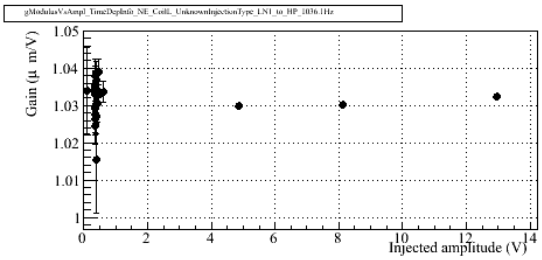

(d) 1036.5 Hz

Figure 20: ***Evolution as function of the signal amplitude of the measured actuation TF ratio (LN1/HP) for the left coil of the NE mirror*** *at four different frequencies. The amplitude in the x-axis is the amplitude of* $V1 : Ca\_NE\_RM\_CoilL$ *during the injections in HighPower mode.*

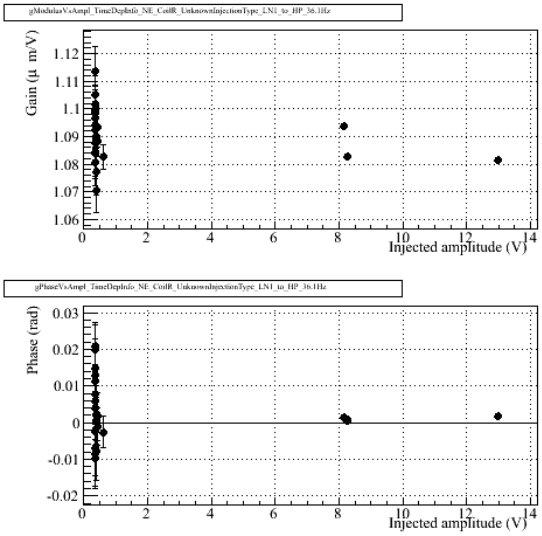

(a) 36.5 Hz

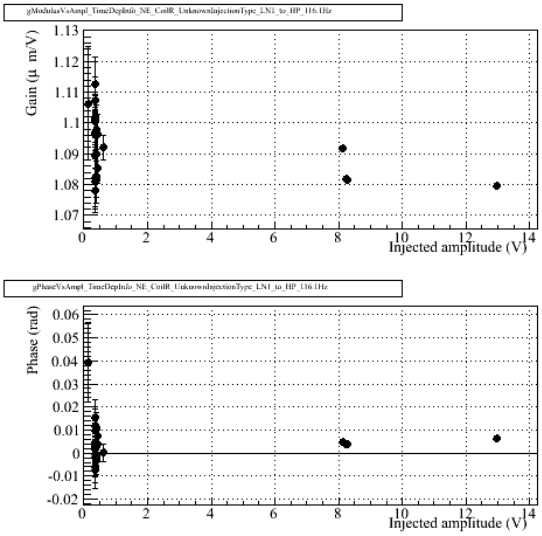

(b) 116.5 Hz

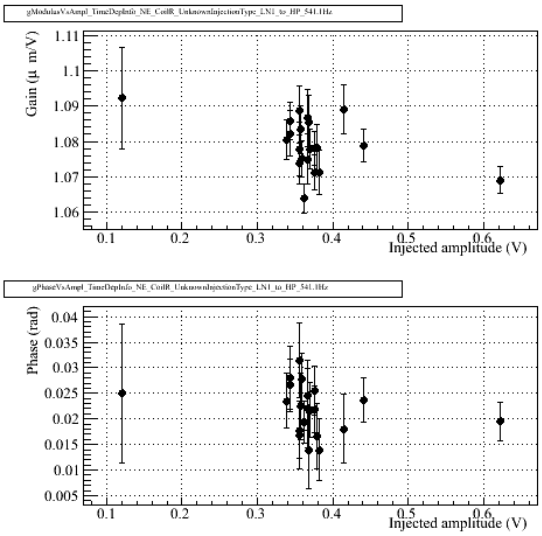

(c) 451.5 Hz

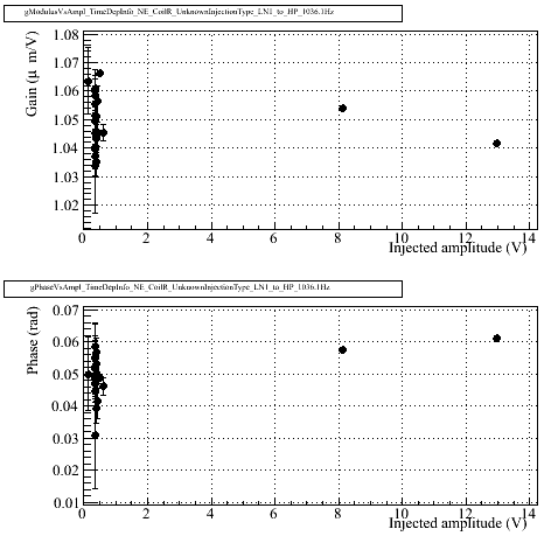

(d) 1036.5 Hz

Figure 21: ***Evolution as function of the signal amplitude of the measured actuation TF ratio (LN1/HP) for the right coil of the NE mirror*** *at four different frequencies. The amplitude in the x-axis is the amplitude of* $V1 : Ca\_NE\_RM\_CoilR$ *during the injections in HighPower mode.*

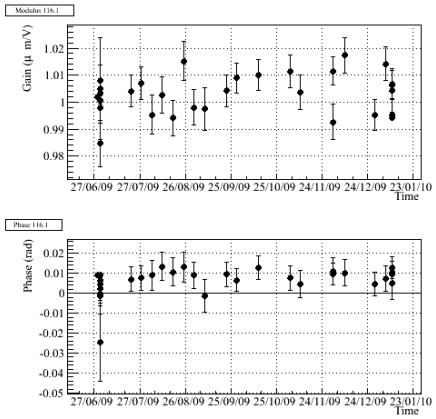

(a) Coil Up, 116.0 Hz

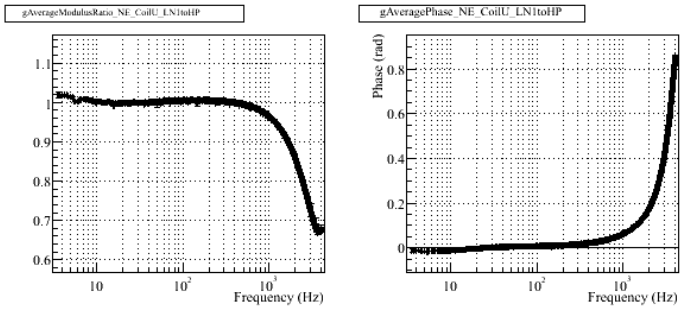

(b) Coil Up, averaged

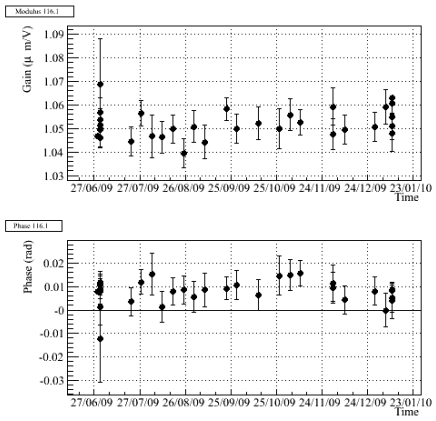

(c) Coil Down, 116.0 Hz

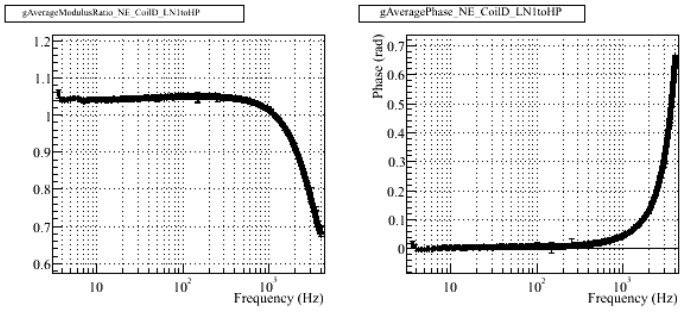

(d) Coil Down, averaged

Figure 22: ***Measured actuation TF ratio (LN1/HP) for the up and down coils of the NE mirror.***

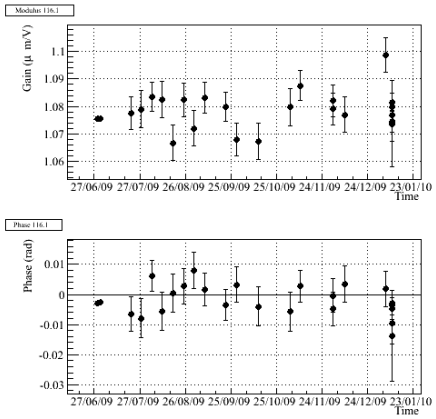

(a) Coil Left, 116.0 Hz

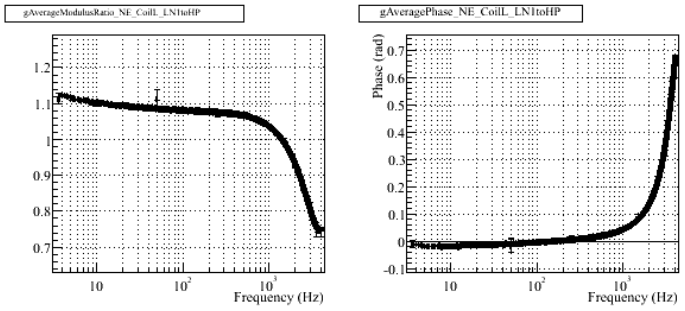

(b) Coil Left, averaged

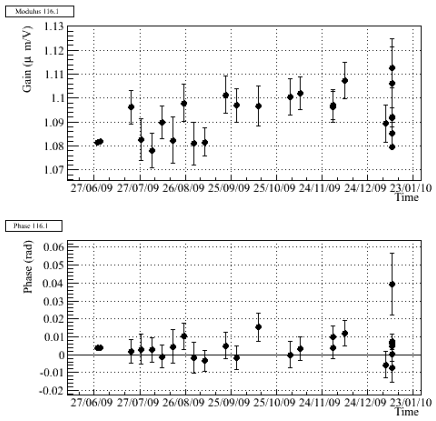

(c) Coil Right, 116.0

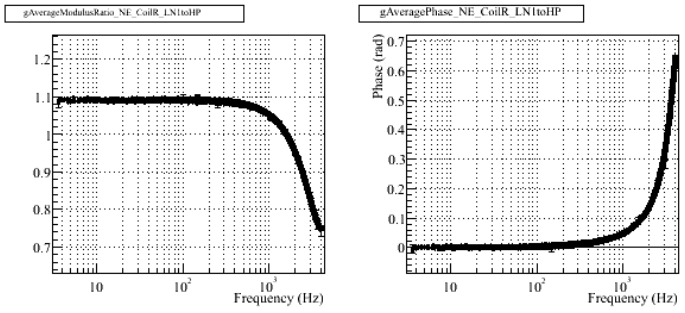

(d) Coil Right, averaged

Figure 23: ***Measured actuation TF ratio (LN1/HP) for the left and right coils of the NE mirror.***

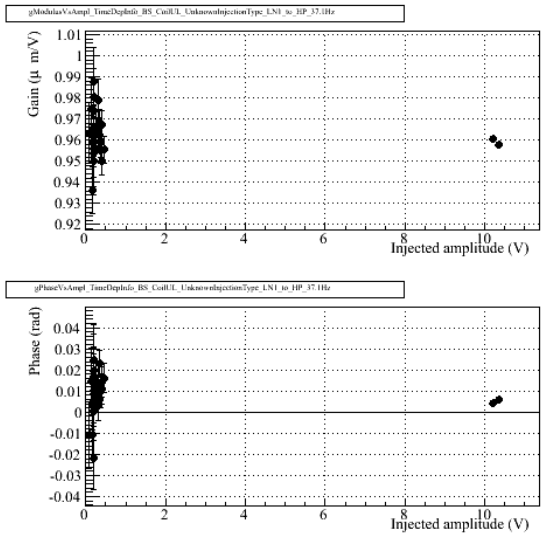

(a) 36.5 Hz

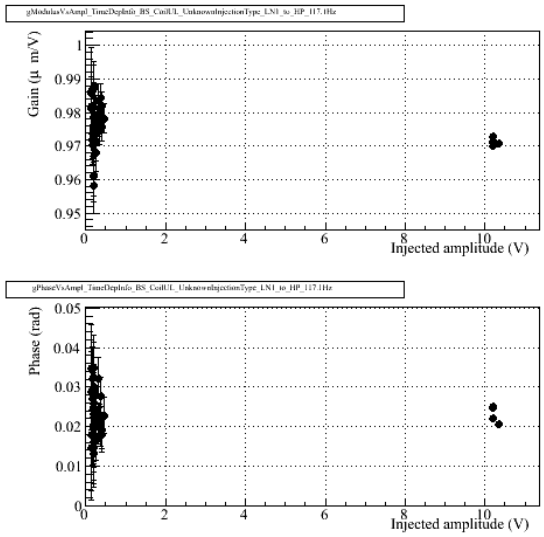

(b) 116.5 Hz

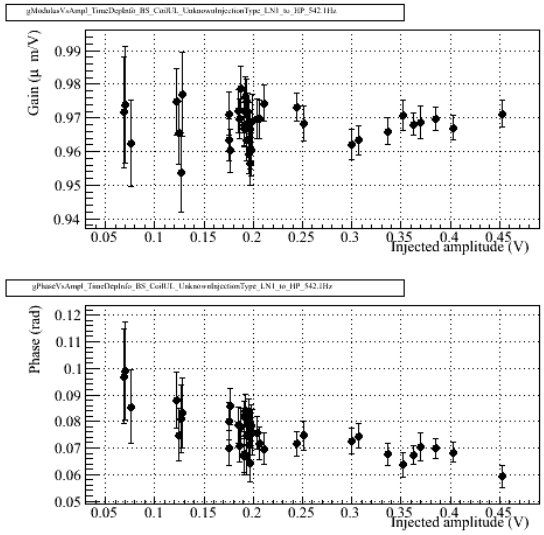

(c) 451.5 Hz

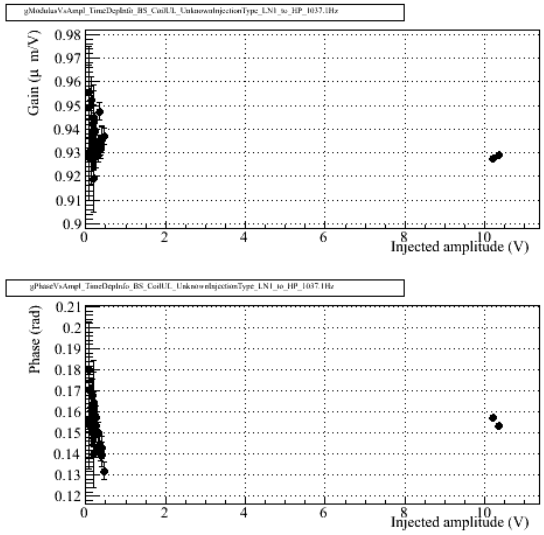

(d) 1036.5 Hz

Figure 24: ***Evolution as function of the signal amplitude of the measured actuation TF ratio (LN1/HP) for the up-left coil of the BS mirror*** *at four different frequencies. The amplitude in the x-axis is the amplitude of* $V1 : Ca\_BS\_RM\_CoilUL$ *during the injections in HighPower mode.*

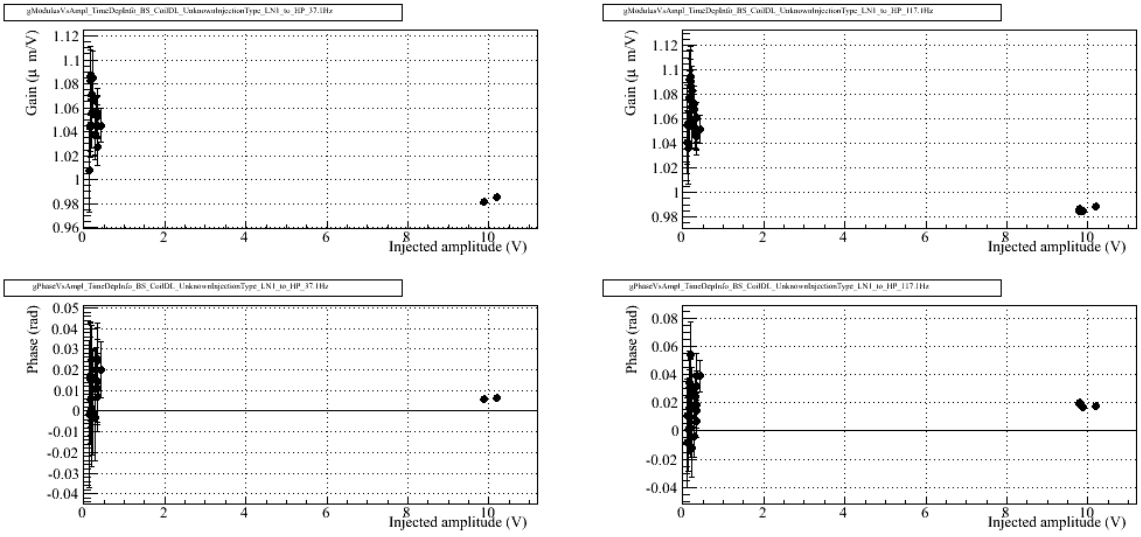

(a) 36.5 Hz

(b) 116.5 Hz

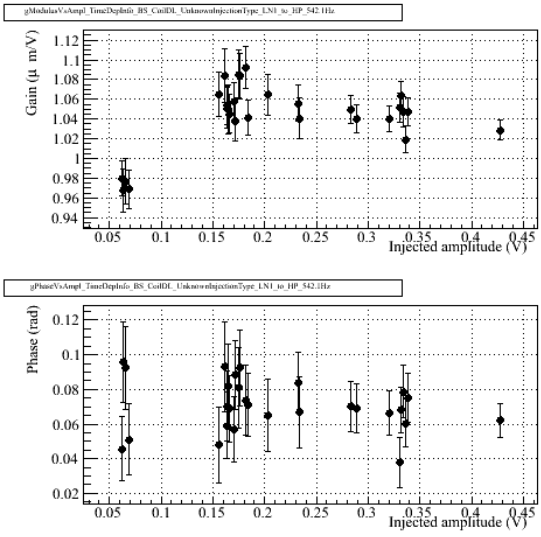

(c) 451.5 Hz

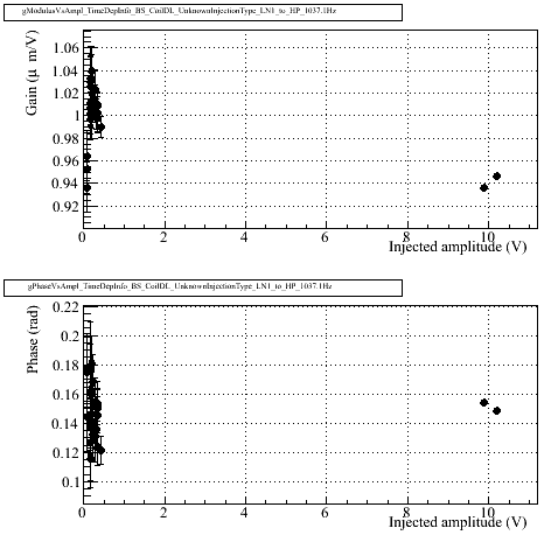

(d) 1036.5 Hz

Figure 25: ***Evolution as function of the signal amplitude of the measured actuation TF ratio (LN1/HP) for the down-left coil of the BS mirror*** *at four different frequencies. The amplitude in the x-axis is the amplitude of* $V1 : Ca\_BS\_RM\_CoilDL$ *during the injections in High-Power mode.*

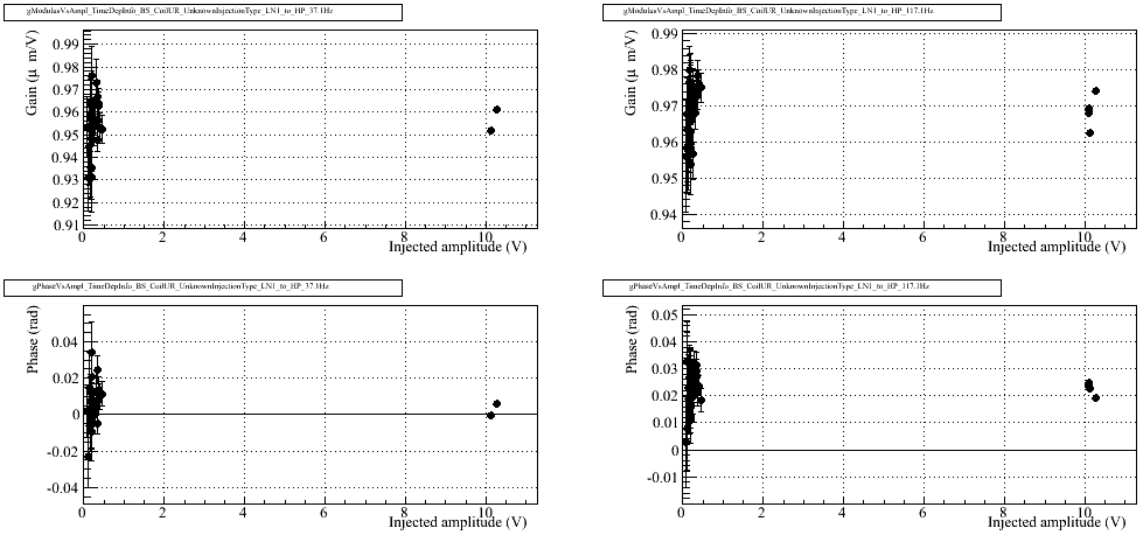

(a) 36.5 Hz

(b) 116.5 Hz

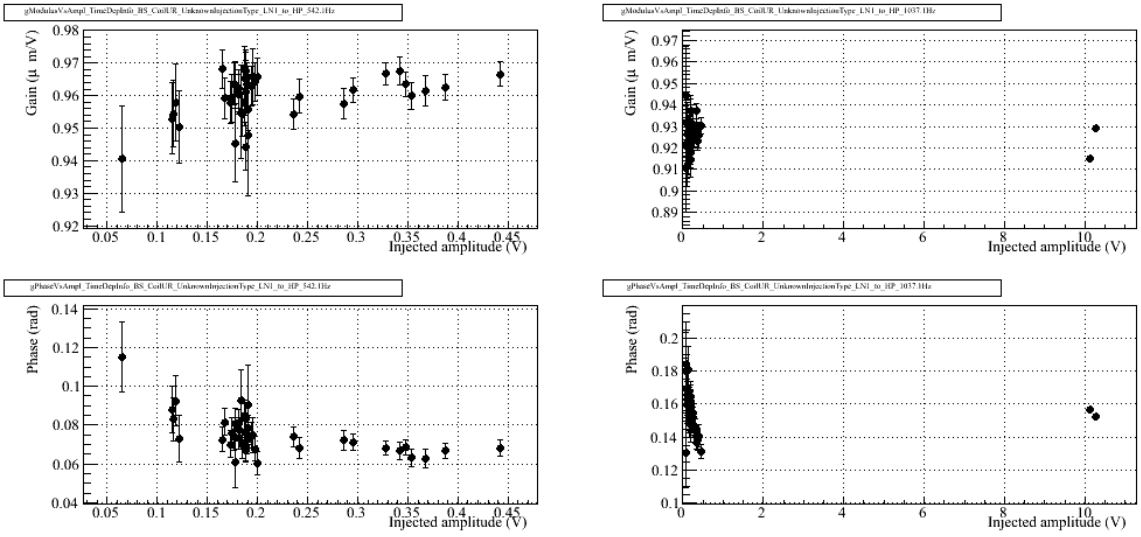

(c) 451.5 Hz

(d) 1036.5 Hz

Figure 26: ***Evolution as function of the signal amplitude of the measured actuation TF ratio (LN1/HP) for the down-left coil of the BS mirror*** *at four different frequencies. The amplitude in the x-axis is the amplitude of* $V1 : Ca\_BS\_RM\_CoilUR$ *during the injections in High-Power mode.*

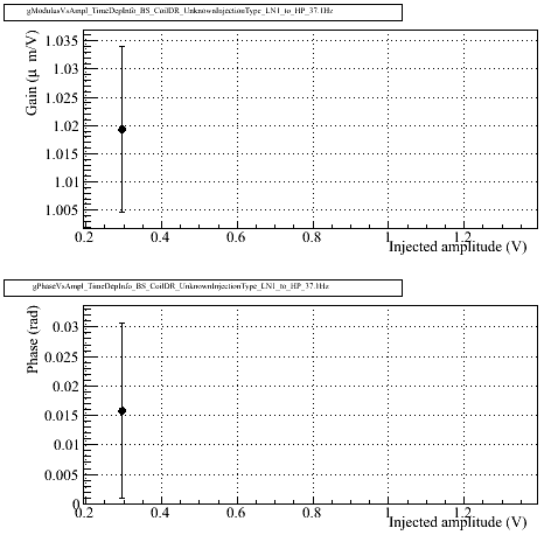

(a) 36.5 Hz

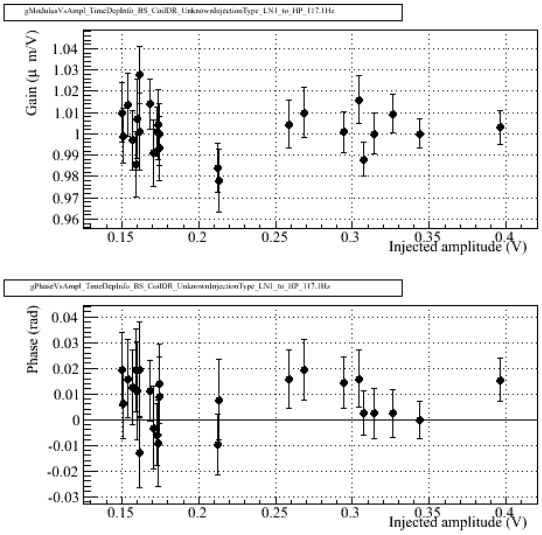

(b) 116.5 Hz

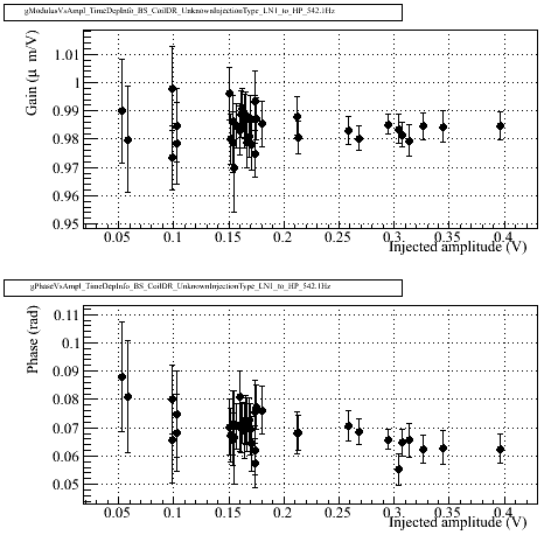

(c) 451.5 Hz

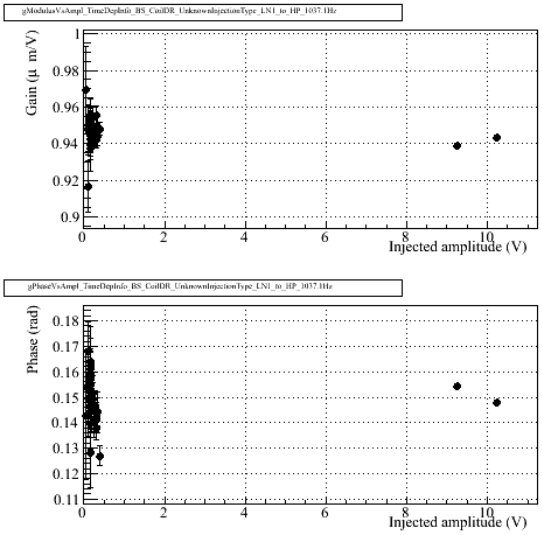

(d) 1036.5 Hz

Figure 27: ***Evolution as function of the signal amplitude of the measured actuation TF ratio (LN1/HP) for the up-left coil of the BS mirror*** *at four different frequencies. The amplitude in the x-axis is the amplitude of* $V1 : Ca\_BS\_RM\_CoilDR$ *during the injections in HighPower mode.*

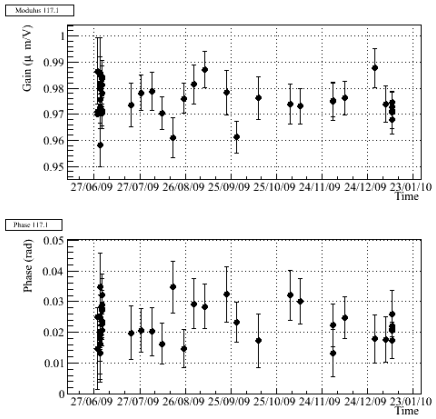

(a) Coil Up-Left, 117.0 Hz

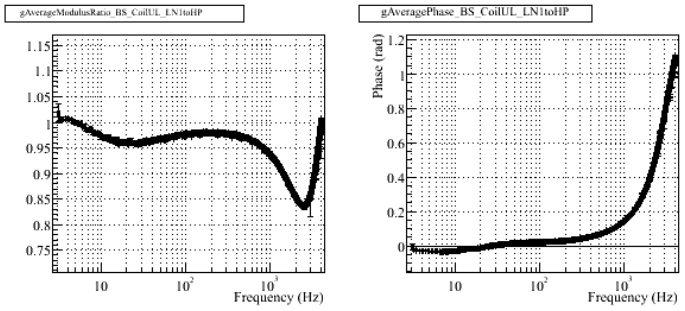

(b) Coil Up-Left, averaged

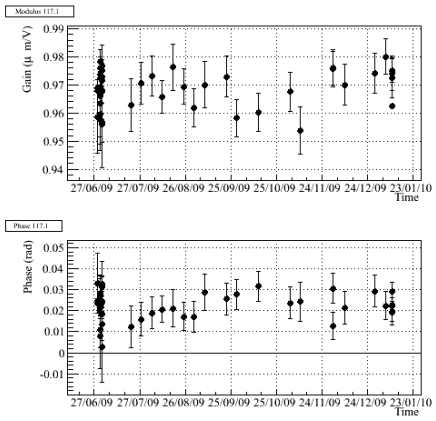

(c) Coil Up-Right, 117.0 Hz

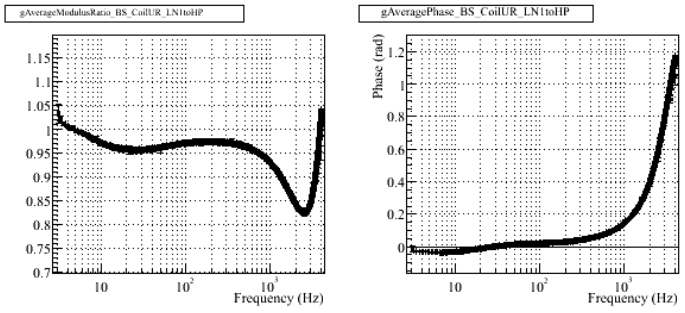

(d) Coil Up-Right, averaged

Figure 28: ***Measured actuation TF ratio (LN1/HP) for the up-left and up-right coils of the BS mirror.***

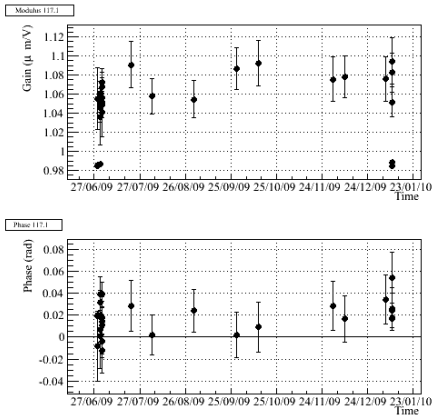

(a) Coil Down-Left, 117.0 Hz

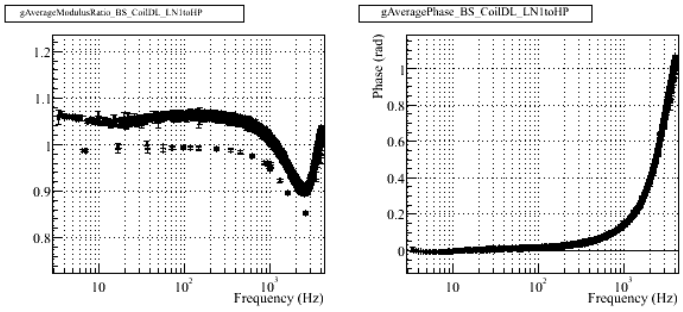

(b) Coil Down-Left, averaged

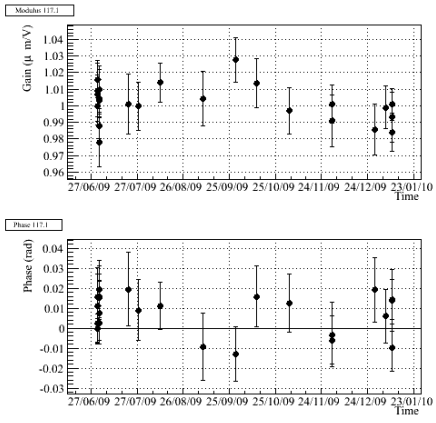

(c) Coil Down-Right, 117.0 Hz

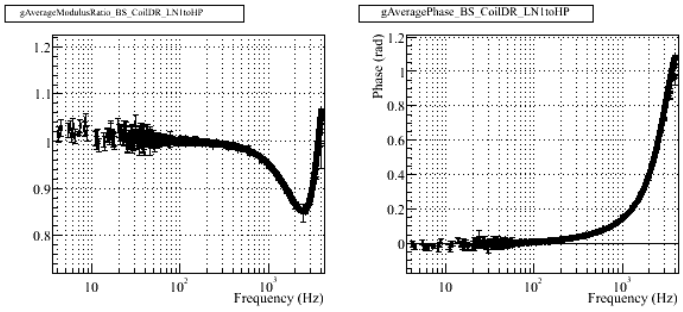

(d) Coil Down-Right, averaged

Figure 29: ***Measured actuation TF ratio (LN1/HP) for the down-left and down-right coils of the BS mirror.***

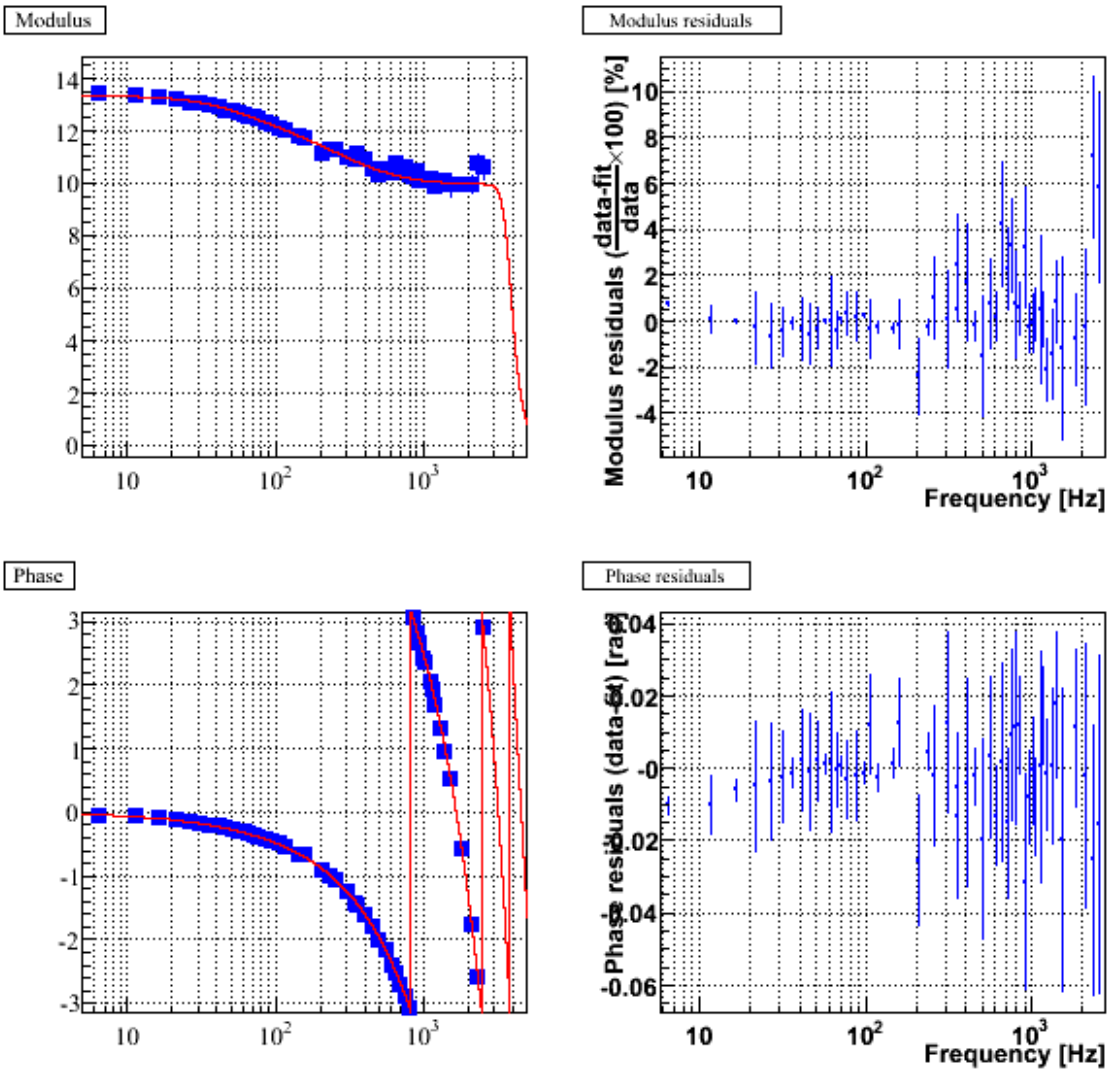

Figure 30: ***Measured actuation of the WE mirror using the U-D coils in LN1 mode****, fitted model and residuals.*

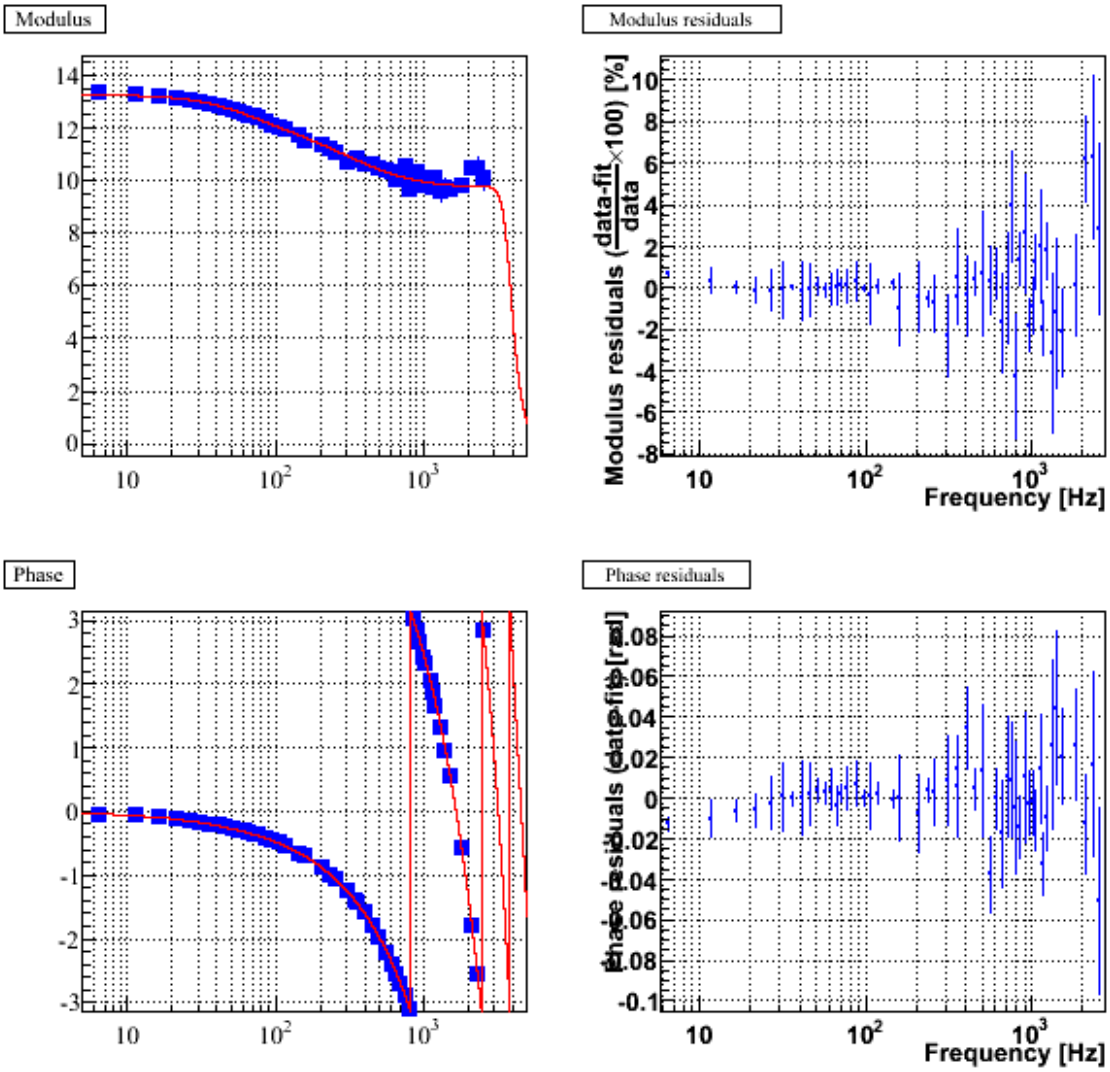

Figure 31: ***Measured actuation of the WE mirror using the L-R coils in LN1 mode****, fitted model and residuals.*

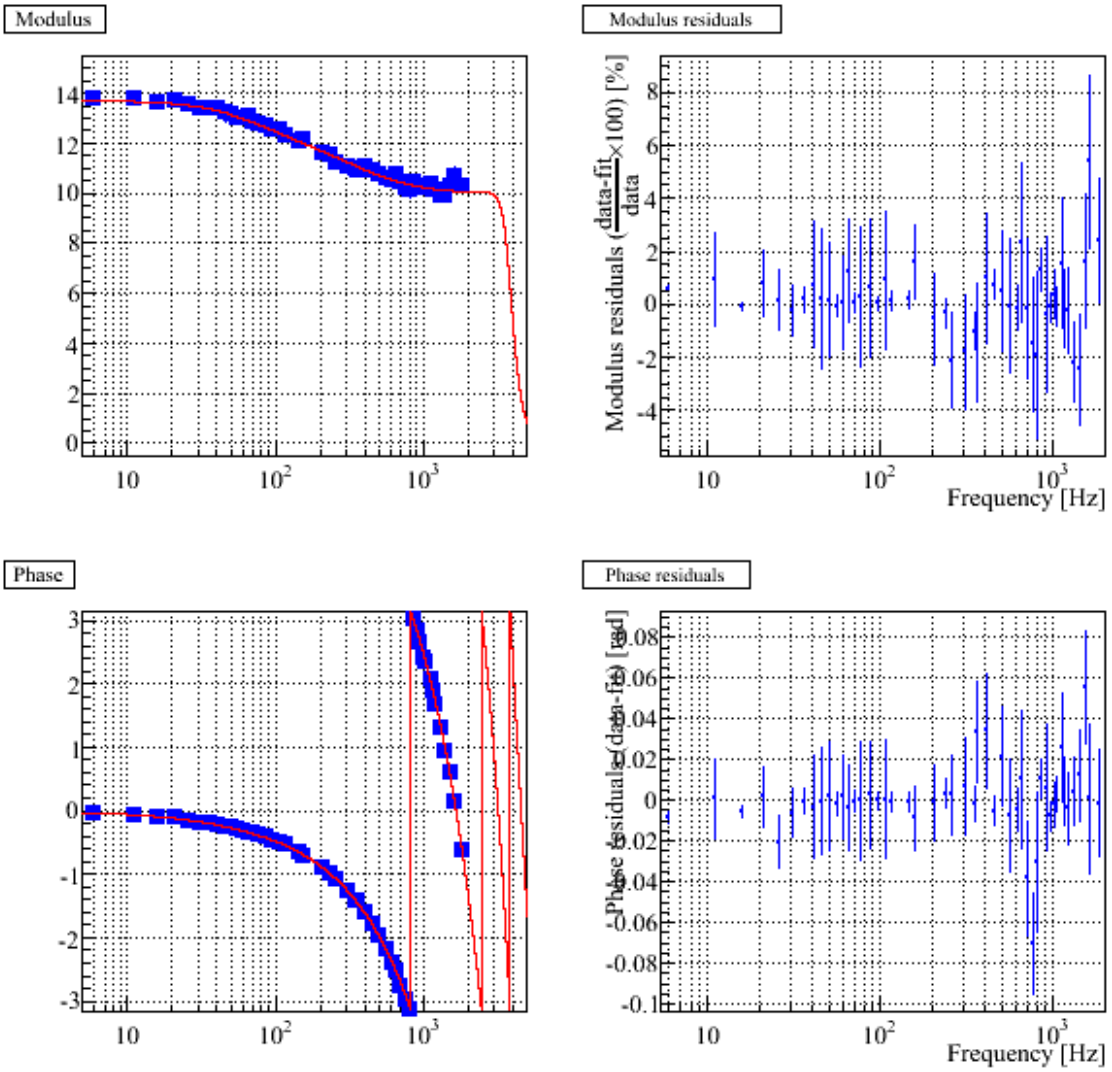

Figure 32: ***Measured actuation of the NE mirror using the U-D coils in LN1 mode****, fitted model and residuals.*

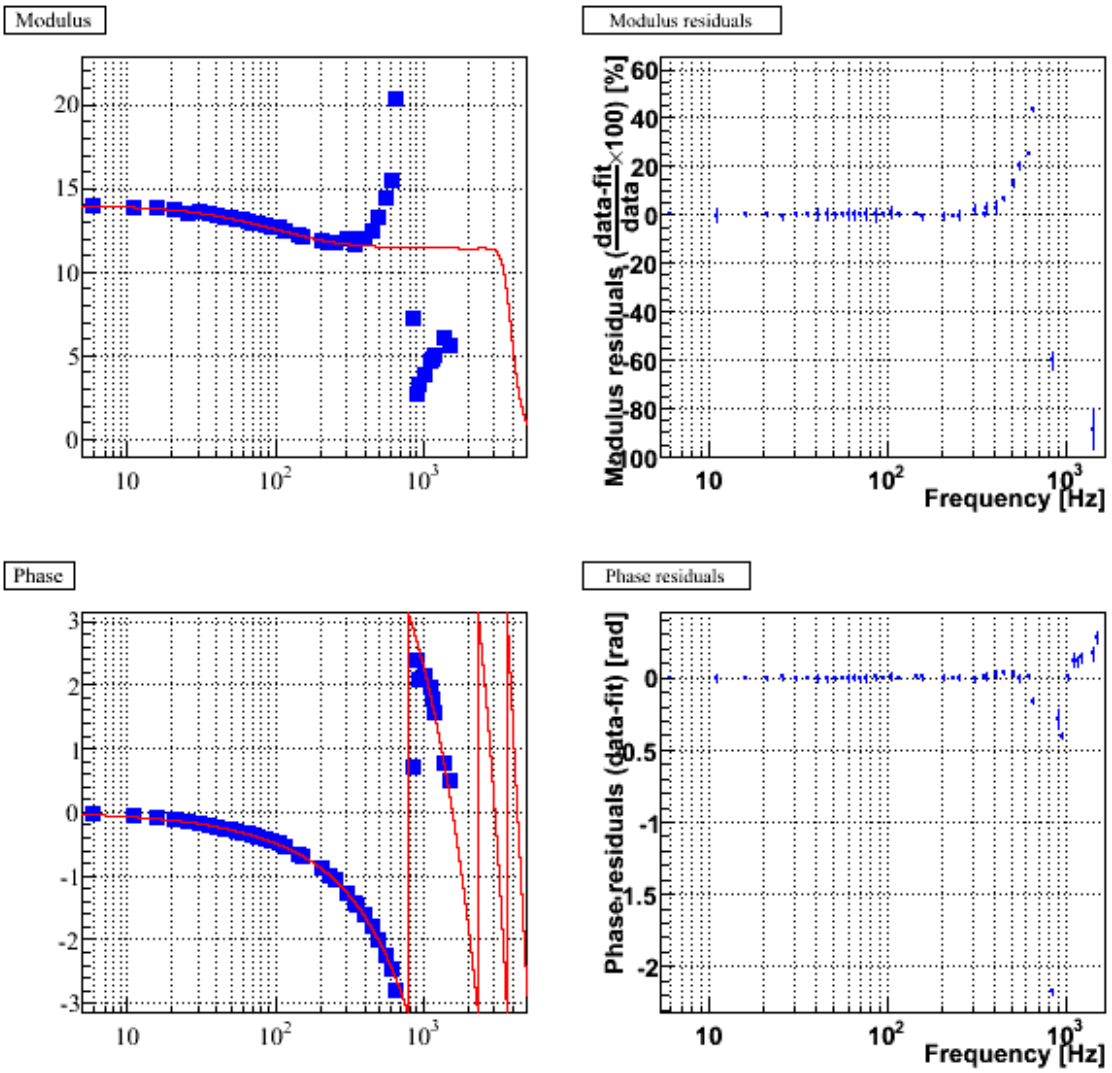

Figure 33: ***Measured actuation of the NE mirror using the L-R coils in LN1 mode****, fitted model and residuals. The data have been fitted below 400 Hz only.*

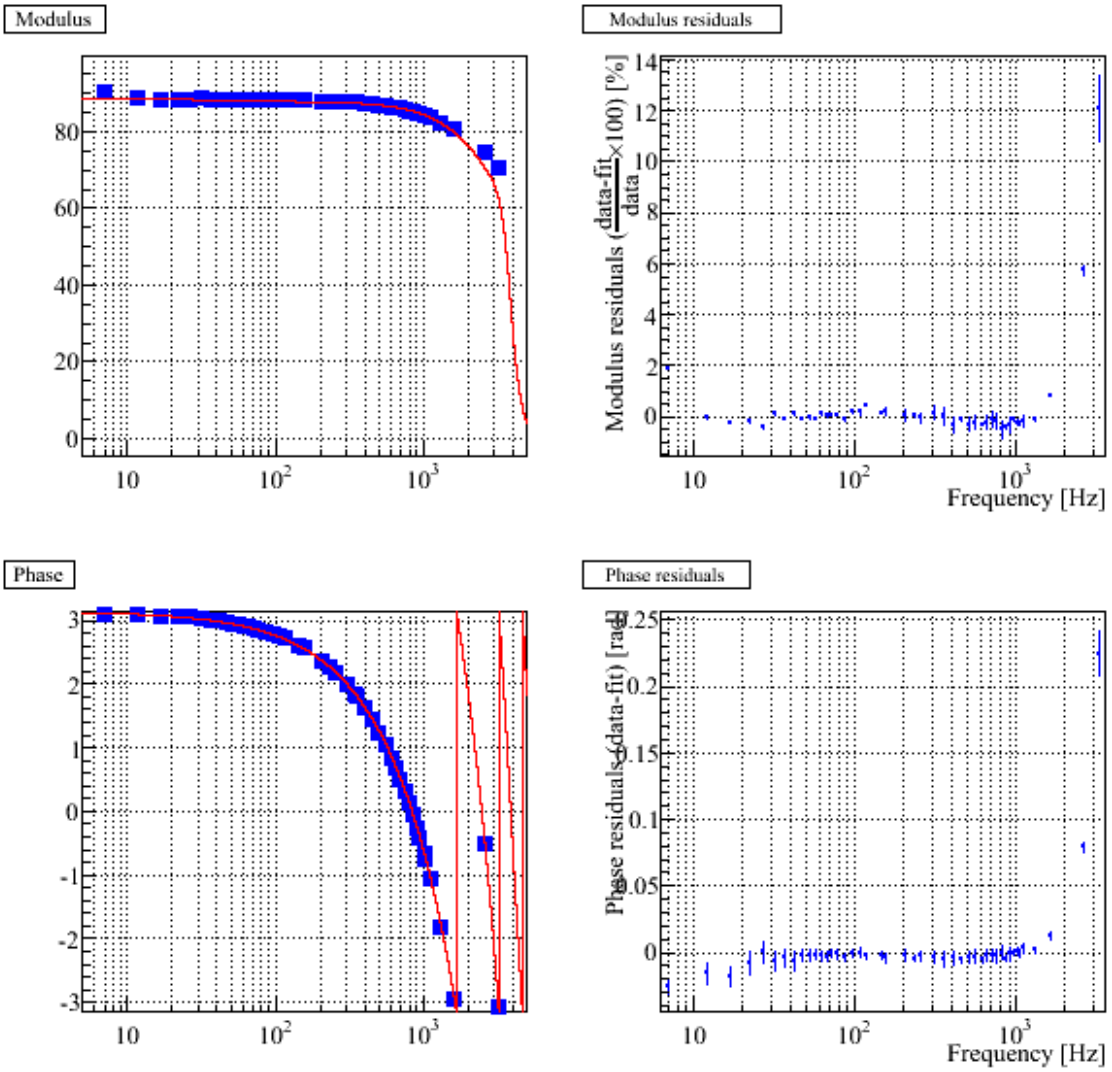

Figure 34: ***Measured actuation of the BS mirror using the four coils in LN1 mode****, fitted model and residuals.*

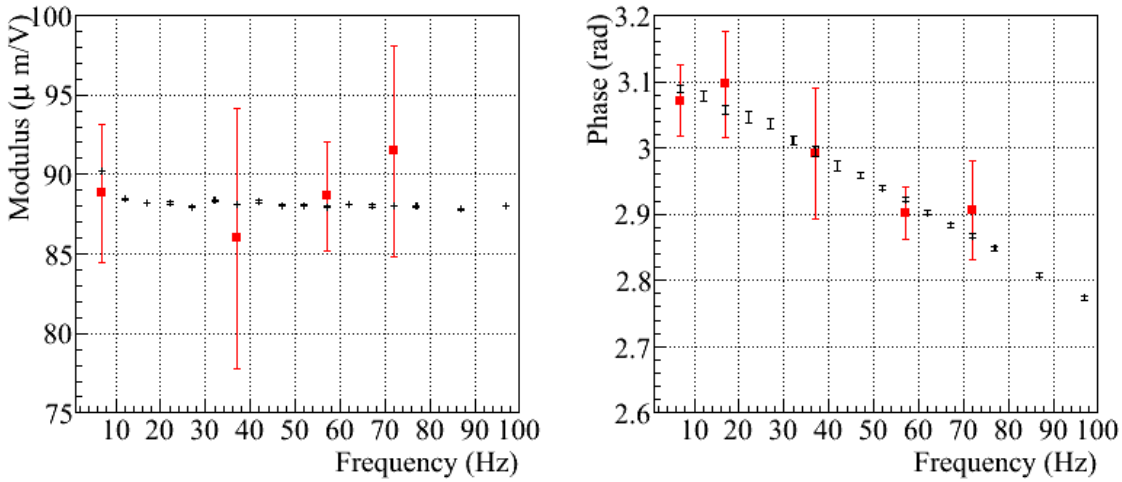

Figure 35: ***Comparison of the measurement of the actuation of the BS mirror using the four coils in LN1 mode****. Black: standard measurements. Red squares: free Michelson measurements.*

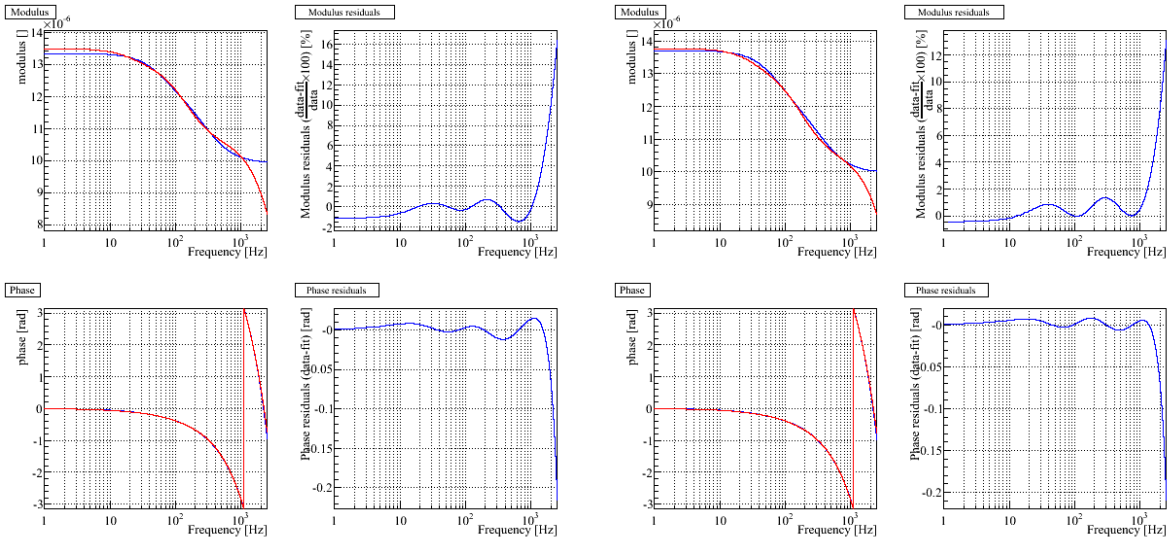

(a) WE, U-D coils, LN1

(b) NE, U-D coils, LN1

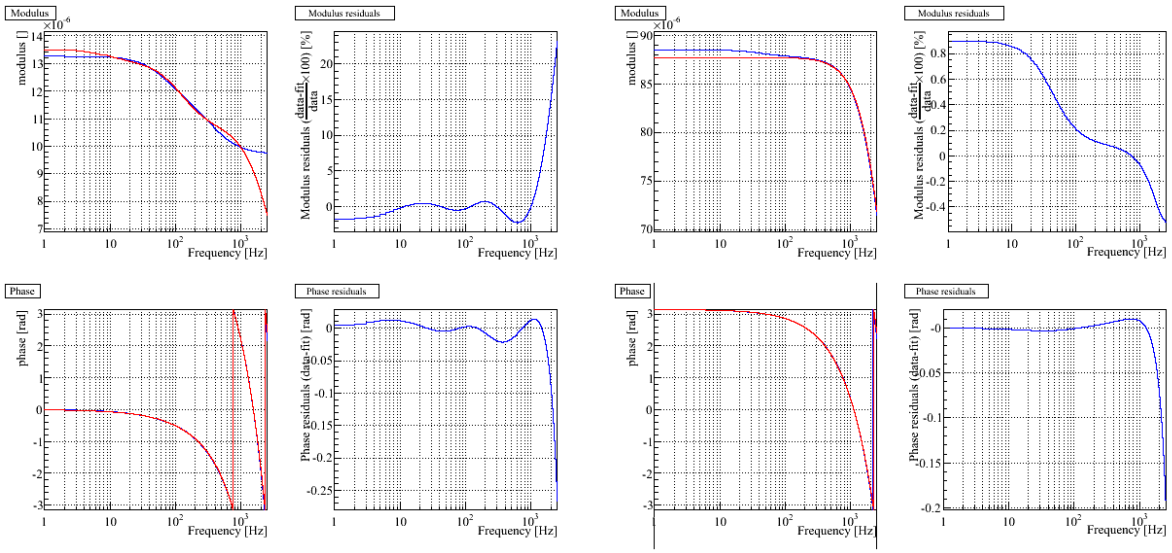

(c) WE, L-R coils, LN1

(d) BS, four coils, LN1

Figure 36: ***Comparison of the mirror actuation parameterizations from note VIR-0576A-09 with the new models.*** *For each suspension, the left plots show the comparison of the TFs: old one in blue, new one in red ; the right plots show the residuals between the models. Note that the pendulum model which is the same in both parameterizations is not shown in the TFs.*

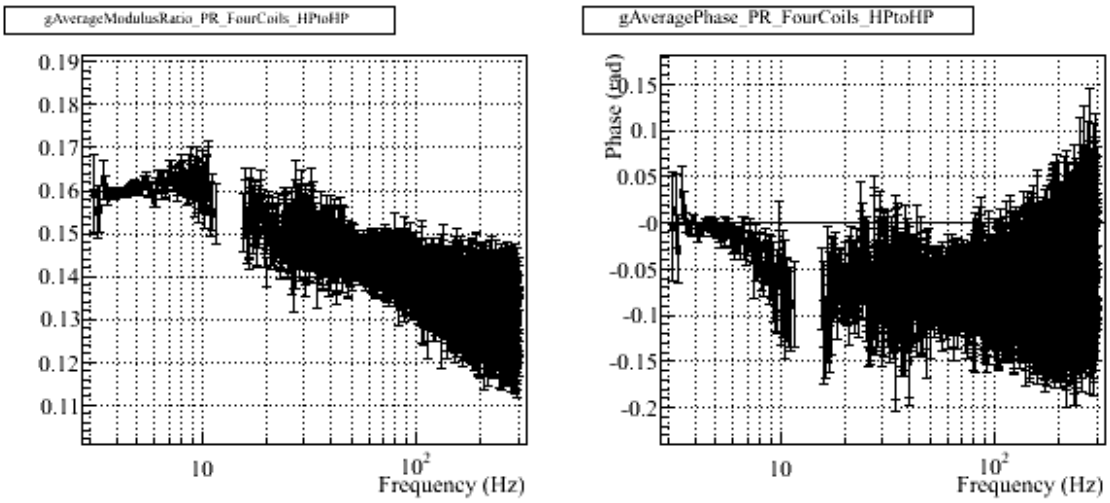

Figure 37: ***Measured ratio of the PR over BS mirror actuation response (in HP mode).***

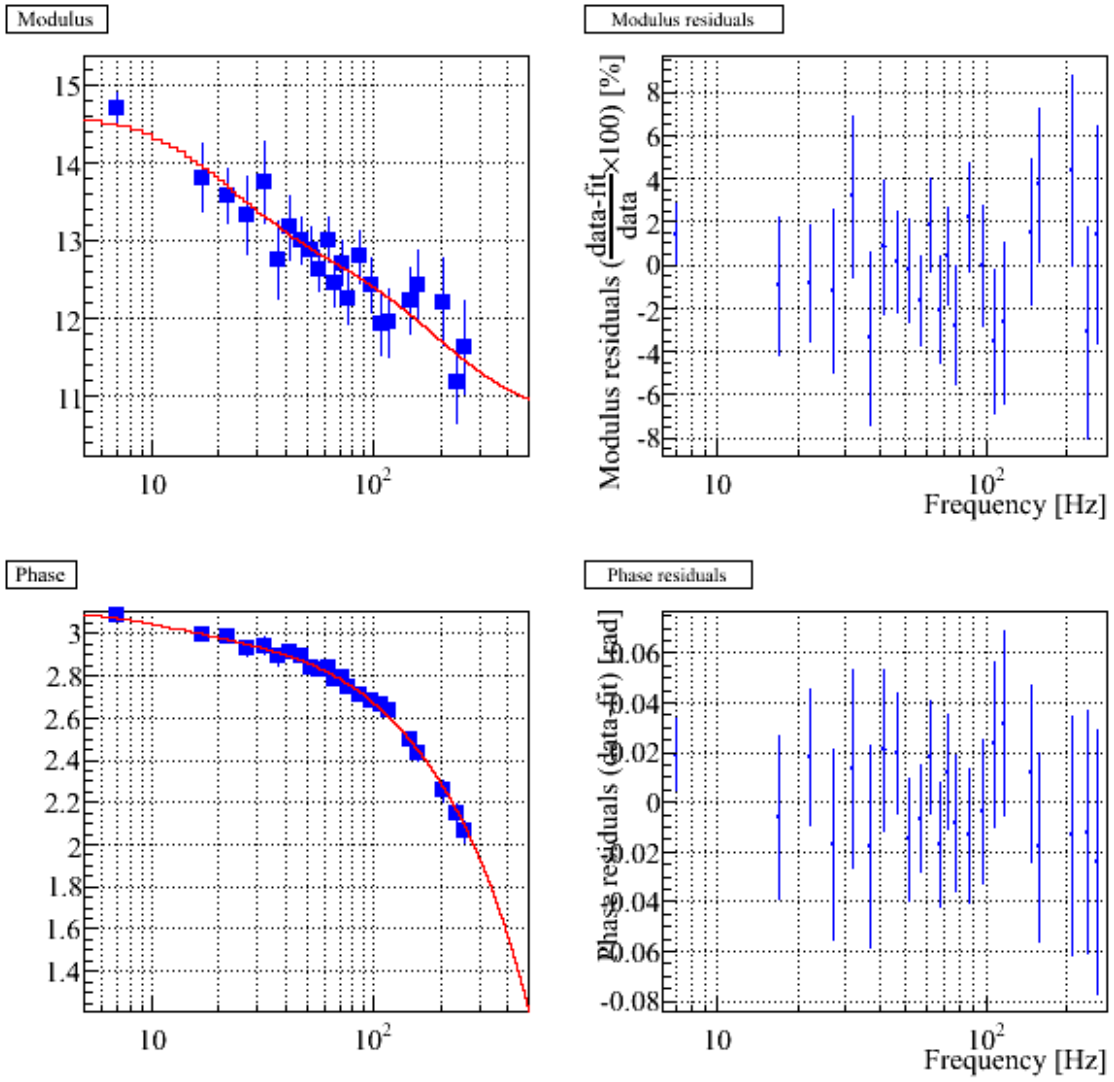

Figure 38: ***Measured actuation TF of the PR mirror actuation****, fitted model and residuals.*

4 Calibration of the marionette actuation

The marionette actuation is defined as the TF (with modulus in m/V) from the correction signal stored in the Virgo data to the induced mirror motion[3]. The time reference for the mirror motion is the GPS time.

In the plots that are shown, the actuation is corrected for a mechanical model of the pendulum[4], defined as **two** 2nd order low-pass filters with $f_0 = 0.6\,\mathrm{Hz}$ and $Q = 1000$.

4.1 Description of the measurements

The calibration of the NE (U-D coils) and WE (U-D coils) mirror actuation in LN1 mode is used as reference to measure the NE and WE marionette actuations.

An intermediate step consists in measuring the Marionette/Mirror TF ratio in step 12. This ratio is then multiplied by the model of the mirror actuation (U-D coils, in LN1 mode) to obtain the marionette actuation. Only the points where the coherence is higher than 90% have been used to estimate the TF ratio.

This analysis assumes that the ITF response (in particular the optical gain) is stable between the two datasets. In principle this is the case since both datasets are taken within 3 minutes. Such data were taken at different times and monitored during VSR2. The stability of the measurements validates this hypothesis.

The injected noise has been white noise from a few Hz to ~ 200 Hz. Different amplitudes of the noise were injected in order to check the linearity of the response. At the end of VSR2 and during post-VSR2 measureements, some lines were added from 5 Hz to 10 Hz in order to better measure actuation at low frequency.

4.2 Calibration of the WE and NE marionettes

The measured ratio of the WE and NE marionette to mirror responses are shown figures 41 and 43 (the mirror and marionette actuations being corrected for their pendulum mechanical model). The monitoring of this ratio as function of time are shown at some frequencies figures 39 and 40.

[3] The marionette longitudinal actuation is done through two coils (left and right). Emphasis filters are set in the DSP for both coil channels in order to compensate for de-emphasis filters used in the coil drivers. The resistance of the coil channel is $R \sim 16.5\,\Omega$ and its inductance is $L \sim 214\,\mathrm{mH}$: the L-R circuit results in a pole $R/(2\pi L)$ around $12 - -13\,\mathrm{Hz}$.

[4] This model is not accurate. A more precise model [7] is two 2nd order low-pass filters at frequencies 0.46 Hz and 0.98 Hz, both with a quality factor of 100.

The obtained marionette TF is shown figures 42 and 44 along with the fitted model and residuals. The fits were performed between 9 Hz and 200 Hz. The fit parameters are given in the table 7. A 2nd order low-pass filter at 1 kHz has been arbitrarily added in order to have a non-divergent TF parameterization. Below 100 Hz, the residuals are flat, lower than 3% in modulus and better than 30 mrad in phase.

Note that the 4 μs timing systematic error are negligible for the marionettes: at 100 Hz, it corresponds to less than 3 mrad phase error.

The new parameterizations are compared to the ones from note VIR-0576A-09 in the figure 46. Between 5 Hz and 100 Hz, the parameterizations agree within 1%/10 mrad in modulus and phase respectively, well below the statistical uncertainties.

4.3 Cross-check of the marionette actuation measurements

The standard way to measure the marionette actuation is done as a combination of measurments of the actuation in HP mode, measurements of the LN1/HP ratio and measurements of the marionette/mirror ratio. In order to cross-check the results, a direct measurement of the WE and NE marionette actuations has been performed using free swinging Michelson data. Due to the limited dynamic of induced mirror motion through the marionette, only some frequencies below ?? Hz have been measured. The results are shown in the figure 45. The free Michelson measurements are only below 5 Hz while the standard measurements start at 5 Hz. However, no strong offset is observed at the limit between both measurements and no systematic error could be highlighted.

4.4 Tables

	WE	NE
Gain (μm/V)	3.037 ± 0.009	15.43 ± 0.04
Raw delay (μs)	$(95.1) \pm 2.8)$	(1406.6 ± 1.8)
Delay (μs)	-54.2 ± 2.8	1257.3 ± 1.8
Φ_0 (rad)	0	0
Pole frequency (Hz)	14.867 ± 0.034	16.568 ± 0.038
Zero frequency (Hz)	0.5016 ± 0.0014	0.3812 ± 0.0011
Pole frequency (Hz)	0.6266 ± 0.0018	0.0991 ± 0.0003
Zero frequency (Hz)	32.36 ± 0.10	36.34 ± 0.12
Pole frequency (Hz)	42.91 ± 0.12	44.93 ± 0.14
Zero frequency (Hz)	$-$	192.71 ± 0.6
Complex zero f_0 (Hz)	-201.66 ± 0.53	-118.237 ± 0.035
Complex zero Q	0.602 ± 0.0010	1.5111 ± 0.0010
2nd order low-pass	$f_0 = 1000\,\mathrm{Hz}$, $Q = 0.7$	
Pendulum	**Two** 2nd order low-pass filters: $f_0 = 0.6\,\mathrm{Hz}$, $Q = 1000$	
χ^2/ndf	4788.89/3727	4437.4/3740

Table 7: ***WE and NE marionette actuation parameterizations.*** *Fit computed from 9 Hz to 200 Hz. The χ^2/ndf of the fits are given. Residuals are within 5% in modulus and 50 mrad in phase up to 150 Hz. The raw delays are the delay measured using the raw delays from the mirror actuation measurements. The delay has been corrected for the PrCa and sensing delays to take as reference the correction channels (i.e. Sc_WE_zMar): delay = raw_delay − 100 − 49.3 μs. Applying these TFs to the correction channels Sc_WE_zMar should enable to estimate the induce motion at absolute GPS time. Note that the error matrix from Minuit is not positively defined ("ERR MATRIX NOT POS-DEF") indicating that the parameter error estimation is not accurate.*

4.5 Figures

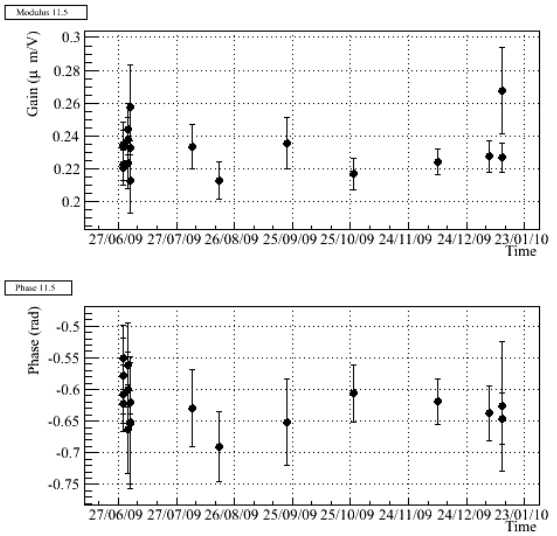

(a) 11.5 Hz

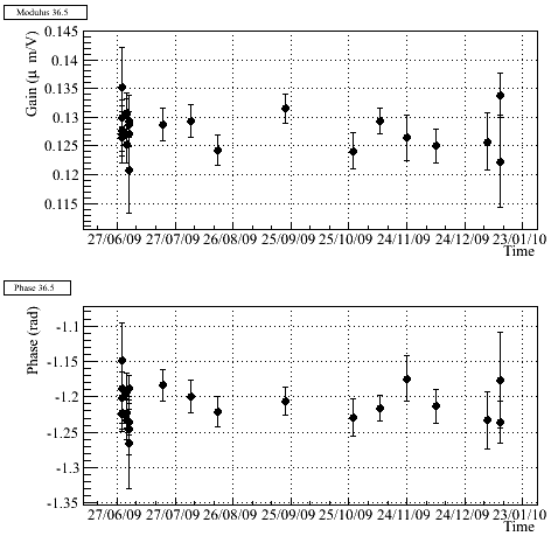

(b) 36.5 Hz

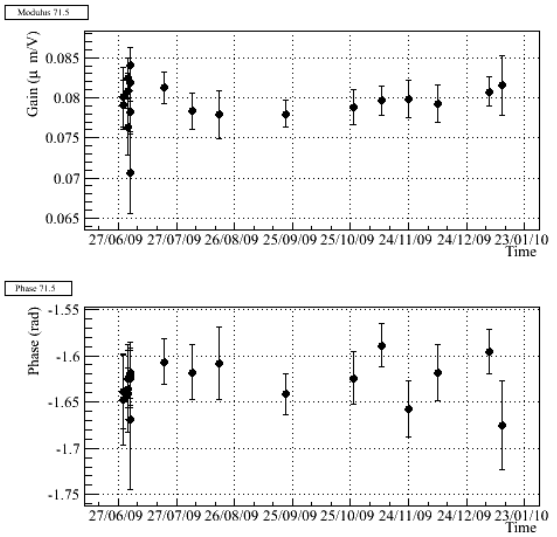

(c) 71.5 Hz

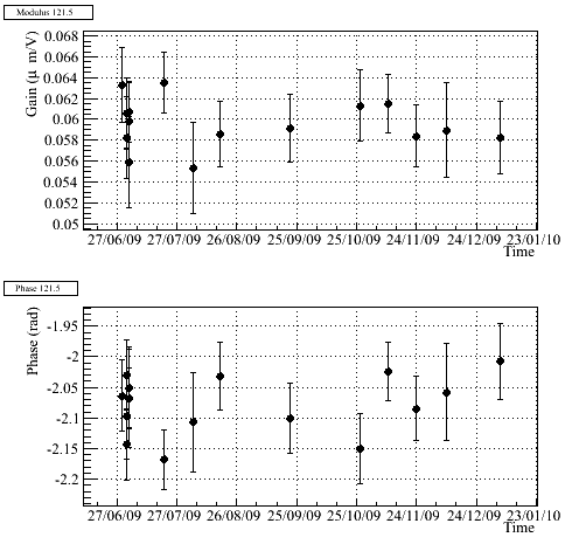

(d) 121.5 Hz

Figure 39: ***Measured WE marionette to mirror actuation (WE, U-D coils) TF ratio as function of time*** *at four different frequencies. The mirror and marionette actuations have been corrected for their pendulum mechanical models.*

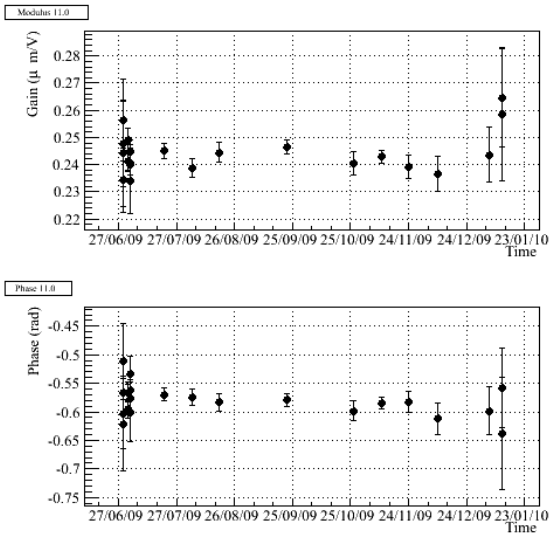

(a) 11.0 Hz

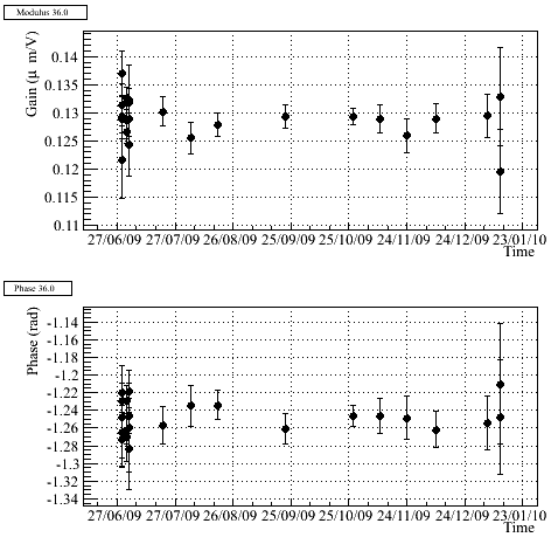

(b) 36.0 Hz

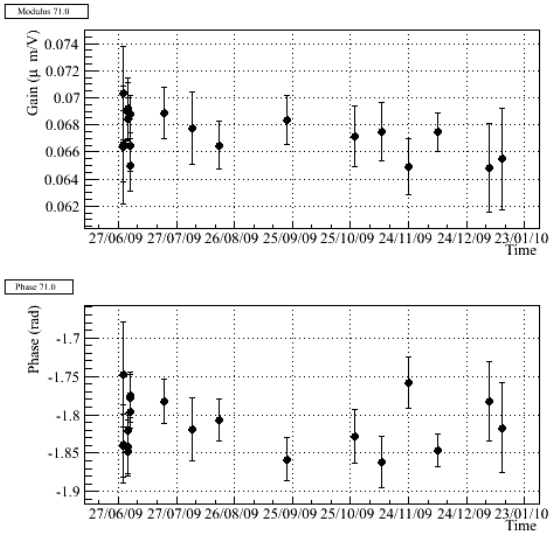

(c) 71.0 Hz

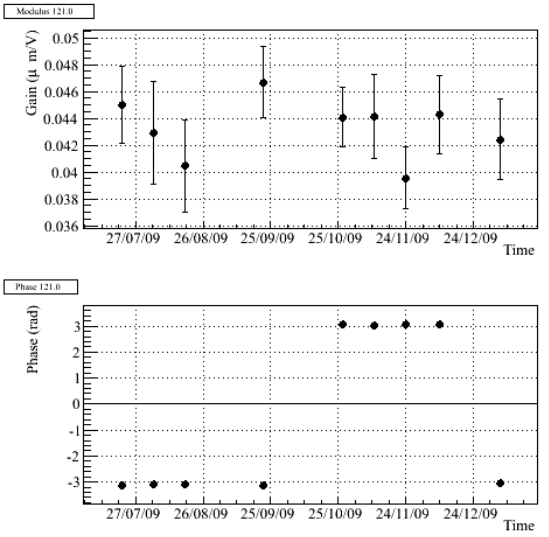

(d) 121.0 Hz

Figure 40: ***Measured NE marionette to mirror actuation (NE, U-D coils) TF ratio as function of time*** *at four different frequencies. The mirror and marionette actuations have been corrected for their pendulum mechanical models.*

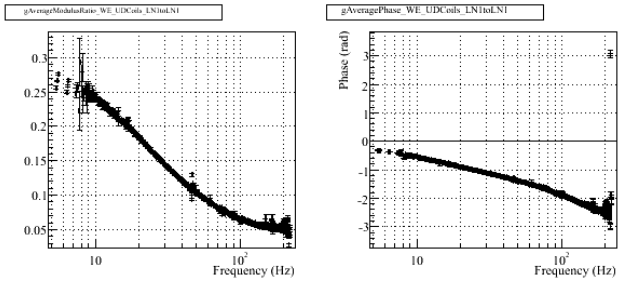

Figure 41: ***Averaged marionette to mirror actuation TF ratio of the WE suspension.*** *The mirror and marionette actuations have been corrected for their pendulum mechanical models.*

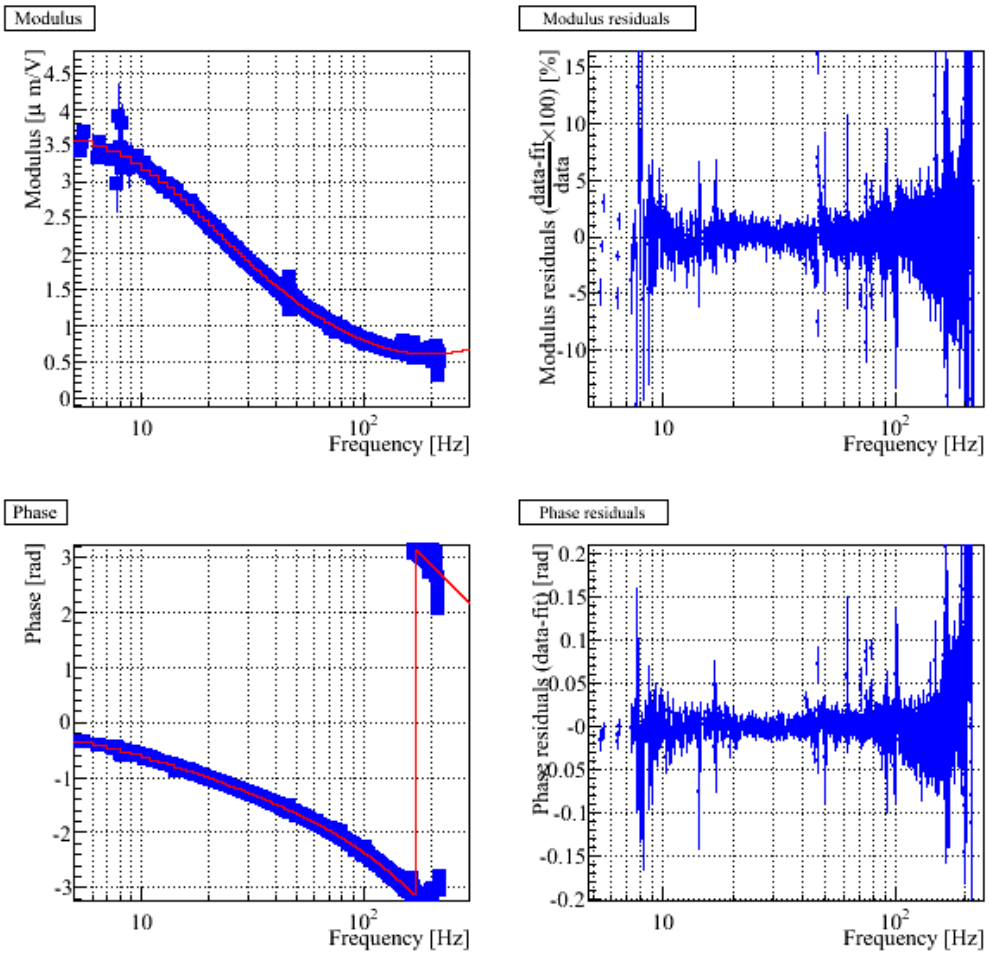

Figure 42: ***Measured WE marionette actuation TF****, fit and residuals.*

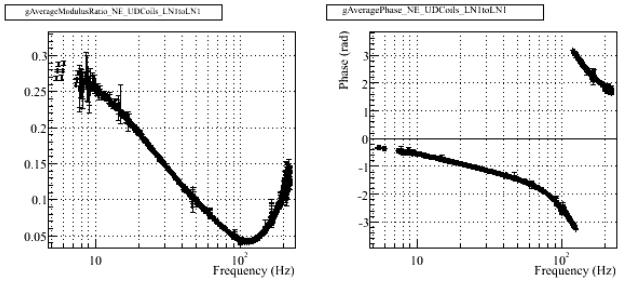

Figure 43: ***Averaged marionette to mirror actuation TF ratio of the NE suspension.***

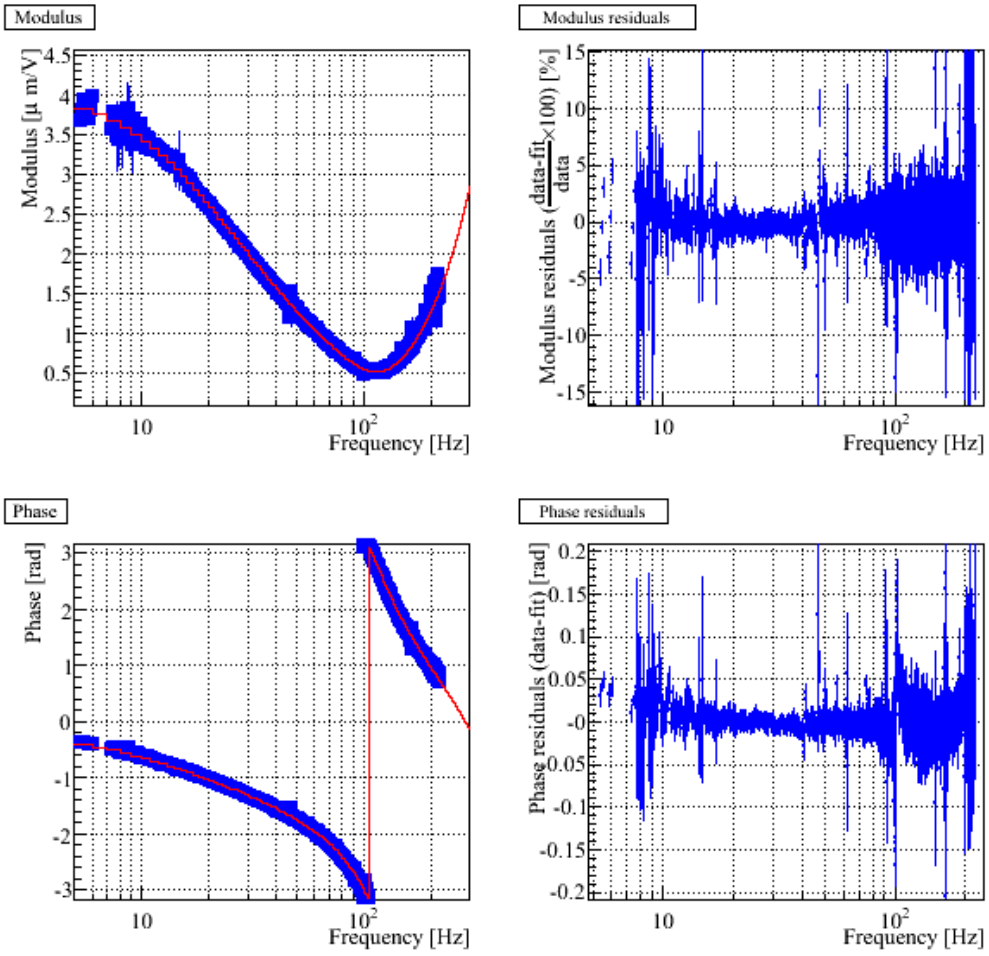

Figure 44: ***Measured NE marionette actuation TF****, fit and residuals.*

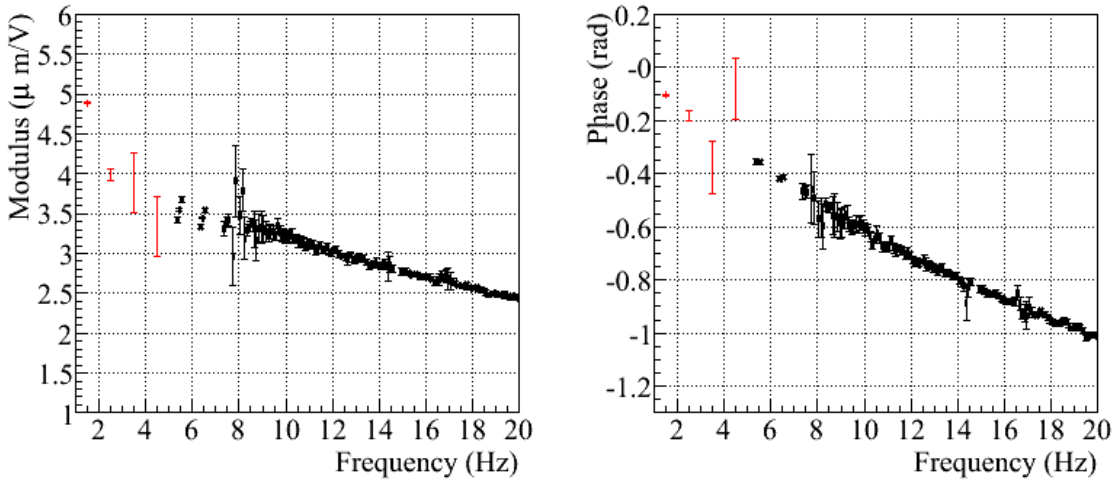

(a) WE marionette

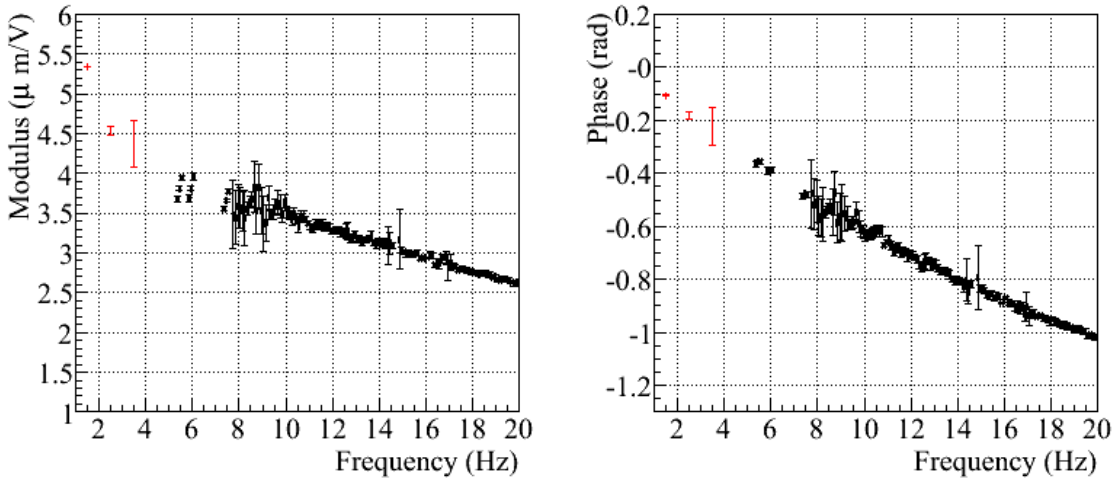

(b) NE marionette

Figure 45: ***Comparison of the marionette actuation measurements****. Black (above 5 Hz): standard measurements. Red (below 5 Hz): free Michelson measurements.*

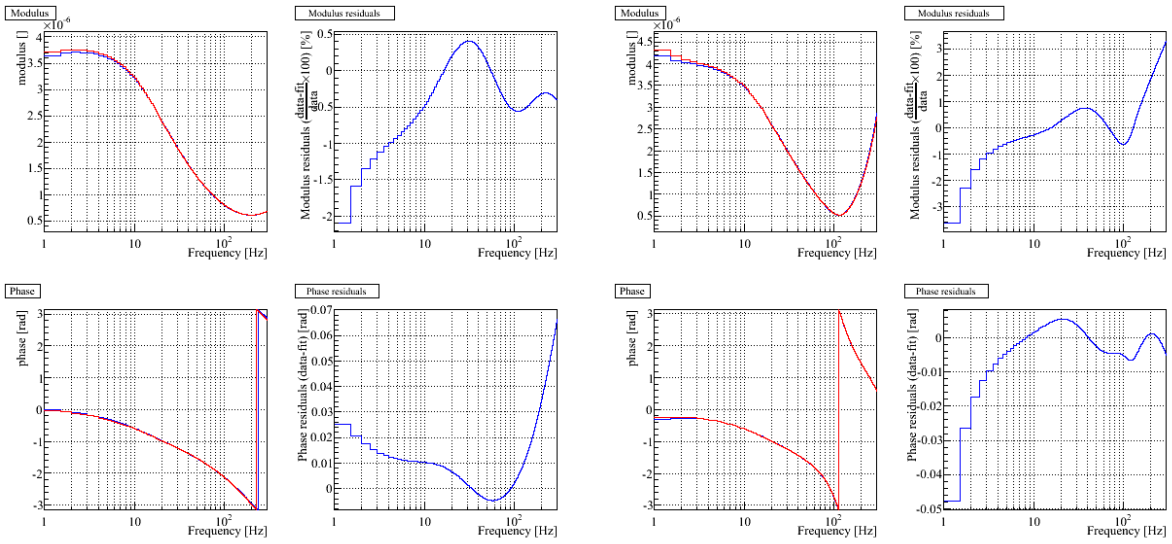

(a) WE, Marionette

(b) NE, Marionette

Figure 46: ***Comparison of the models from note VIR-0576A-09 (blue) with the new models (red)*** *For each comparison, the left plots show the comparison of the TFs: old one in blue, new one in red; the right plots show the residuals between the models. Note that the fixed 2nd order low-pass filter and pendulum model which are the same in both parameterizations are not shown in the TFs.*

5 VSR2 hardware injection models

Hardware injections (HI) of fake gravitationnal wave signals have been performed during VSR2 through the WE mirror actuation through the L-R coils in LN1 mode. The HI process takes as input the $h(t)$ signal to be injected in the ITF and computes the excitation signal to be sent to the WE mirror actuation (Ca_WE_zMirLR). This conversion is done using the inverse TF of the mirror actuation response.

Two different parameterizations for the actuation response have been used during VSR2: one from pre-run calibration, used up to October 20th 2009 around 9h20 UTC, and another one from the note VIR-0576A-09 used afterwards[5]. Their parameters are given in the table 8. The TFs are compared to the final parameterization from this note (see table 5) in the figure 47.
For the first part of the run, the signals were injected with amplitudes within 2% of the final parameterization below 2 kHz but with phases offsets between 100 mrad and -350 mrad.
For the second part of the run, the signals were injected with amplitudes within 2% below 1 kHz, but 18% too low at 2 kHz. The phase was correct within 20 mrad up to ~ 1.5 kHz. The phase error of 90 mrad at 2 kHz is equivalent to an advance of the injected signals of 7 μs.

	Up to 20/10/2009	From 20/10/2009
Gain (μm/V)	13.39	13.51
Delay (μs)	681.9	594.1
Φ_0 (rad)	π	π
Pole frequency (Hz)	26.8	9.557
Zero frequency (Hz)	28.6	9.896
Pole frequency (Hz)	220.7	116.5
Zero frequency (Hz)	286.1	142.0
Pole frequency (Hz)	-	2450
Pendulum	Pole frequency: 0.6 Hz Pole frequency: 0.6 Hz	Low-pass frequency: 0.6 Hz Quality factor: 1000

Table 8: ***WE (L-R coils) mirror actuation parameterizations used for the hardware injections during VSR2****. The sign of the injections were checked before the start of VSR2: it resulted in the use of a phase of π in the TF.*

[5] see logbook entry 25294

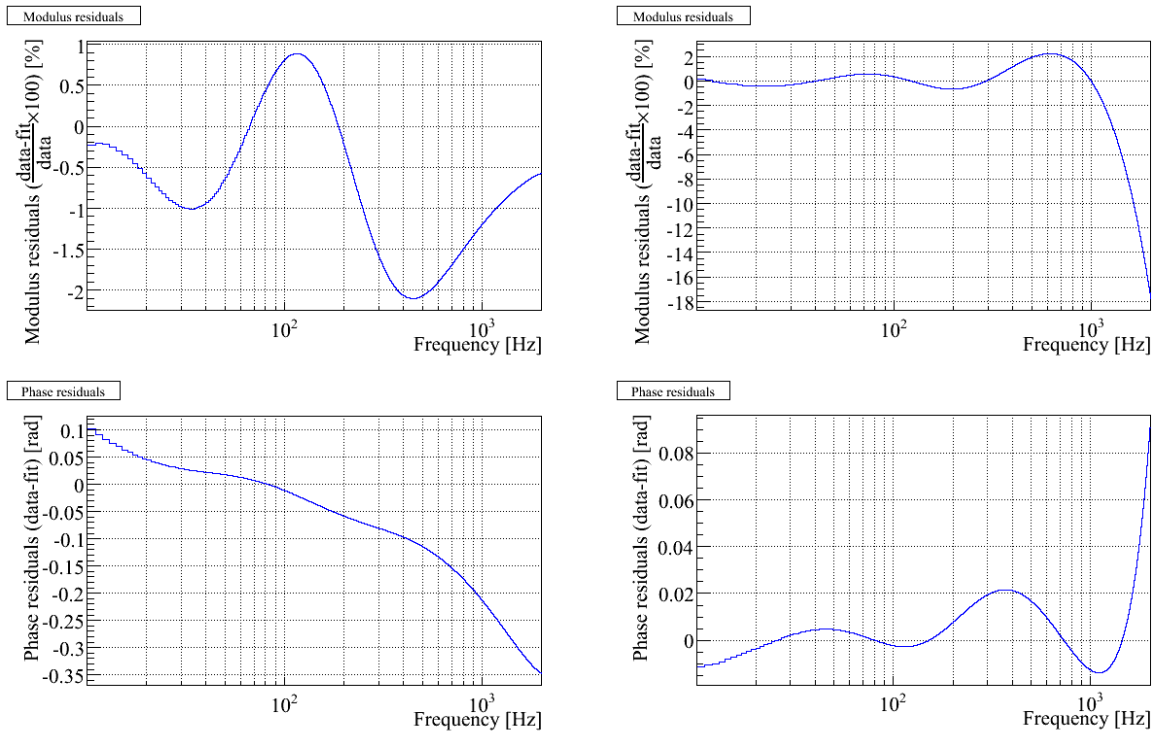

(a) July to October 20th 2009

(b) October 20th 2009 to January 2010

Figure 47: ***Residuals between the models used for the hardware injections during VSR2 and the model of this note.*** *Modulus:* $(G_{HImodel} - G_{CurrentModel})/G_{CurrentModel}$. *Phase:* $\Phi_{HImodel} - \Phi_{CurrentModel}$. *Actuation of the WE mirror using the L-R coils, in LN1 mode.*

6 Conclusions

The full VSR2 calibration has been computed with data from June 28th to January 15th 2010, including pre- and post-run measurements and run periodic measurements.

The **dark fringe readout** has been calibrated (see note [1]), the timing being related to the absolute GPS time. The timing has been computed from the time series stored in FrVect setting the value of sample i at the time $startX[0] + i \times dx[0]$. The 20 kHz dark fringe channel models, given in the table 1, are **understood from 1 Hz to 10 kHz within systematic errors of** ± 4 μs**.** The 40 kHz dark fringe channel models, given in the table 2, are understood from 1 Hz to 10 kHz within systematic errors of $\pm 3\%$ in modulus, ± 30 mrad in phase and ± 4 μs. The time stability of the sensing response have been checked.

The **BS, WE and NE mirror actuations in LN1 mode have been measured from 5 Hz to** $\sim$**2 kHz**. The parameterizations are given in the tables 4 for the controls and 5 for the hardware injections. The delays are related to the absolute GPS time. Up to 2 kHz, the statistical errors are well below 1%/10 mrad in modulus and phase respectively at the frequencies that where monitored during the run, while they are of a the order of 3%/30 mrad for the post-run additionnal measurements. **The model residuals below 1 kHz are of the order of 2%/20 mrad. They increase up to 5%/50 mrad around 2 kHz to 2.5 kHz** (note that at 2 kHz, 50 mrad is equivalent to a delay of 4 μs).

The monitoring data repeated every week or two weeks during VSR2 show that the parameters have been stable within statistical errors from July 3rd 2009 to January 8th 2010. The errors are dominated by systematic errors coming from the LN1/HP measurements: some coils show few percents dependence of the modulus ratio on the injected noise amplitude. **The systematic errors on the mirror actuation response in LN1 mode are estimated to** $\sim$**3% on modulus. Observed phase variations are below** 10 μs**.** It is possible that an additionnal uncertainty of $\sim$ 5 μs and $\sim$ 10 μs should be added to the WE actuation when using the L-R and U-D coils respectively.

The **PR mirror actuation response** has been measured below 300 Hz after the run. The parameterization is given in the table 6. **Up to 300 Hz, the statistical errors and residuals are within 5%/50 mrad in modulus and phase respectively.** Systematic errors are expected to be negligible.

The **marionette actuation responses have been measured from 6 Hz to** $\sim$**200 Hz.** The parameterizations are given in the table 7 for WE and NE. The delays are related to the absolute GPS time. The monitoring data during VSR2 and the different injected amplitudes did not show any variations within statistics. **The systematic errors include the errors from the mirror actuation – ~2% in modulus and ~20 mrad in phase – and the residuals of the parameterizations: better than 3%/30 mrad, up to 100 Hz** for WE

and NE marionettes.

References

[1] L. Rolland *Calibration status in September 2009* (2009) VIR-076A-09.

[2] S. Vilalte *Circuit Design of a Pulse Generator* (2003) VIR-0572A-09.

[3] N. Letendre, A. Masserot, B. Mours, *Virgo+ timing deployement* (2009) VIR-073B-08.

[4] B. Caron et al., Astroparticle Physics 10, 369-386 (1999), *SIESTA, a time domain, general purpose simulation program for the VIRGO experiment.*

[5] L. Rolland, F. Marion, B. Mours, *Mirror motion reconstruction for free swinging Michelson data* (2008) VIR-0112A-08.

[6] L. Rolland, F. Marion, B. Mours, *Mirror and marionette actuation calibration for VSR1* (2008) VIR-015A-08.

[7] D. Huet, *Actuation noise projection for Virgo+MS* (2009) VIR-0573A-09.

[8] A. Gennai, private discussion 2006

A Some data points

A.1 Free Michelson measurements: example of WE, U-D coils, in HP mode

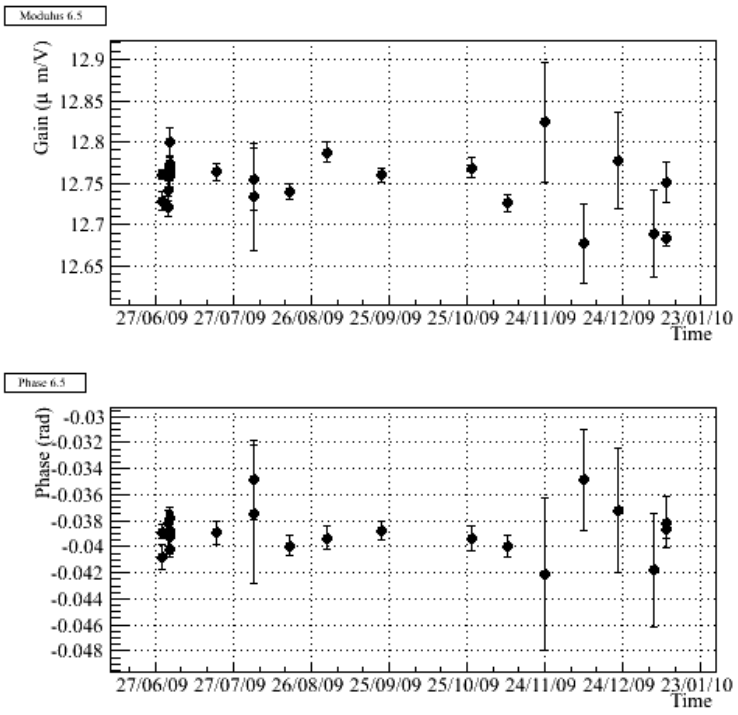

Figure 48: ***Time variations of the actuation of WE, U-D coils, in HP mode, at 6.5 Hz, during VSR2*** *from free swinging Michelson data. The χ^2 probability of the modulus for being a constant is very low (2×10^{-16}) but the observed variations are lower than 0.7%.*

Freq (Hz)	Modulus (μm/V)	Phase (rad)	$P(\chi^2)$ modulus	$P(\chi^2)$ phase
6.5	12.751 ± 0.00622	-0.03905 ± 0.0005044	2×10^{-16}	0.8482
11.5	12.678 ± 0.0755	-0.06925 ± 0.006202	0.1961	0.5290
16.5	12.676 ± 0.0125	-0.09629 ± 0.001018	0.00033	0.9370
21.5	12.580 ± 0.195	-0.1248 ± 0.01630	0.9422	0.7525
26.5	12.481 ± 0.174	-0.1506 ± 0.01446	0.1010	0.3304
31.5	12.446 ± 0.130	-0.1764 ± 0.01086	0.8426	0.5882
36.5	12.406 ± 0.0293	-0.2012 ± 0.002418	0.02557	0.9058
41.5	12.314 ± 0.165	-0.2228 ± 0.01244	0.3369	0.5813
46.5	12.216 ± 0.160	-0.2497 ± 0.01457	0.00041	0.02132
51.5	12.171 ± 0.110	-0.2710 ± 0.009309	0.3070	0.8494
56.5	12.127 ± 0.0102	-0.2945 ± 0.0008765	5.4×10^{-5}	0.02664
61.5	12.064 ± 0.231	-0.3149 ± 0.01785	0.2648	0.7838
66.5	11.958 ± 0.0987	-0.3400 ± 0.008639	0.2478	0.3840
71.5	11.944 ± 0.0153	-0.3603 ± 0.001324	0.06957	0.2031
76.5	11.927 ± 0.112	-0.3829 ± 0.009115	0.05149	0.9403
86.5	11.778 ± 0.124	-0.4246 ± 0.01086	0.5216	0.7444
96.5	11.685 ± 0.0145	-0.4634 ± 0.001281	0.5952	0.1616
106.5	11.543 ± 0.143	-0.4903 ± 0.01243	0.3671	0.1346
116.5	11.464 ± 0.0294	-0.5432 ± 0.002393	0.1636	0.5355
146.5	11.230 ± 0.0258	-0.6554 ± 0.002375	0.6636	0.2411
156.5	11.200 ± 0.114	-0.6819 ± 0.01019	0.06346	0.2290
206.5	10.658 ± 0.175	-0.9087 ± 0.01641	0.6184	0.6058
236.5	10.747 ± 0.0372	-0.9913 ± 0.003564	0.4061	0.07859
256.5	10.806 ± 0.193	-1.0711 ± 0.01800	0.7669	0.2584
306.5	10.523 ± 0.224	-1.2404 ± 0.02274	0.07297	0.9017
351.5	10.440 ± 0.0574	-1.4214 ± 0.005621	0.003366	0.2345
356.5	10.617 ± 0.242	-1.4478 ± 0.02165	0.04723	0.3853
406.5	10.438 ± 0.271	-1.6200 ± 0.02715	0.02670	0.8192
451.5	10.147 ± 0.0634	-1.7822 ± 0.006467	0.8420	0.7141
506.5	9.942 ± 0.256	-1.9985 ± 0.02613	0.8970	0.7079
556.5	10.123 ± 0.198	-2.1578 ± 0.02057	0.7739	0.5485
616.5	10.014 ± 0.110	-2.3907 ± 0.01140	0.4169	0.4678
656.5	10.422 ± 0.295	-2.5235 ± 0.02589	0.02005	0.9458
706.5	10.188 ± 0.185	-2.7231 ± 0.01885	0.9514	0.03180

Table 9: Continued...

Freq (Hz)	Modulus (μm/V)	Phase (rad)	$P(\chi^2)$ modulus	$P(\chi^2)$ phase
756.5	10.286 ± 0.218	-2.8832 ± 0.02243	0.5177	0.6260
806.5	10.004 ± 0.234	-3.0639 ± 0.02441	0.4077	0.7374
851.5	9.994 ± 0.117	3.0547 ± 0.01200	0.1590	0.2848
906.5	10.272 ± 0.276	2.8087 ± 0.02815	0.9271	0.1910
951.5	9.925 ± 0.107	2.6649 ± 0.01111	0.8472	0.9607
1016.5	9.956 ± 0.127	2.4309 ± 0.01319	-1.0000	-1.0000
1036.5	10.005 ± 0.113	2.3470 ± 0.01169	0.9569	0.2325
1116.5	10.055 ± 0.322	2.0592 ± 0.02996	0.4296	0.005590
1156.5	10.025 ± 0.120	1.9247 ± 0.01214	0.008415	0.09614
1216.5	9.844 ± 0.130	1.6826 ± 0.01392	0.5213	0.8941
1316.5	9.965 ± 0.190	1.3081 ± 0.01999	0.3084	0.9295
1416.5	10.253 ± 0.183	0.9474 ± 0.01853	0.8209	0.6132
1516.5	10.120 ± 0.394	0.5295 ± 0.04032	0.1012	0.7981
1816.5	10.403 ± 0.204	-0.5930 ± 0.02040	0.7951	0.7625
2116.5	10.799 ± 0.362	-1.7776 ± 0.03487	0.4608	0.7798
2316.5	11.948 ± 0.450	-2.6026 ± 0.03557	0.01267	0.09272
2516.5	12.092 ± 0.526	2.8766 ± 0.04501	-1.0000	-1.0000

Table 10: ***Data points measured for the WE actuation using the U-D coils in HP mode*** *(from all the free swinging Michelson data of VSR2 from June 2009 to January 2010). For every frequency, the time-average modulus and phase are given. These values are given averaging all the VSR2 measurements. The χ^2 probabilities of the data with the average value are also given in order to check their compatibility with a constant during the run (-1 means that a single point was measured).*

B Filter definitions

The definitions of the different filters used in the calibration prameterizations are given in this appendix[6].

B.1 Simple pole (1st order low-pass filter)

A 1sr order low-pass filter at frequency f_p is described as:

$$H(f) = \frac{1 - \mathrm{j}x}{1 + x^2}$$

where $x = \frac{f}{f_p}$.

The frequency f_p should be positive to have a stable filter.

B.2 Simple zero

A zero at frequency f_0 is described as:

$$H(f) = 1 + \mathrm{j}x$$

where $x = \frac{f}{f_0}$.

B.3 2nd order low-pass filter (complex pole)

A 2nd order low-pass filter at frequency f_0 with quality factor Q is described by:

$$H(f) = \frac{-f_0^2(f^2 - f_0^2) - \mathrm{j}\frac{f_0^3 f}{Q}}{(f^2 - f_0^2)^2 + (\frac{f f_0}{Q})^2}$$

The frequency f_0 should be positive to have a stable filter.

B.4 Complex zero

A complex zero at frequency f_0 with quality factor Q is described as the inverse of a 2nd order low-pass filter:

$$H(f) = \frac{1}{\frac{-f_0^2(f^2 - f_0^2) - \mathrm{j}\frac{f_0^3 f}{Q}}{(f^2 - f_0^2) + (\frac{f f_0}{Q})^2}}$$

[6] Their is a sign issue for the pole and zero definitions as they are used here but these formula are what was used to fit the TFs.

B.5 8th order Butterworth filter

A 8th order Butterworth filter with a cut-off frequency f_0 is defined as:

$$H(s) = \frac{1}{(s^2 + 0,3902s + 1)(s^2 + 1,1111s + 1)(s^2 + 1,6629s + 1)(s^2 + 1,9616s + 1)}$$

where $s = \mathrm{j} \times \frac{f}{f_0}$.

B.6 Anti-alias of the DAC in the mirror actuation

The parameters[7] of the DAC anti-alias are given in the table 3. The absolute sign of z_1, p_1, p_2, p_4, p_6 and p_7 is important (they are all negative). The sign of the other pulsations is not important in the computation since they are squared.

The TF can be written $H(w) = \frac{N(w)}{D(w)}$ with:

$$\begin{aligned}
N(w) &= (1 - \mathrm{j}\frac{\omega}{z_1}) && (3)\\
&\times(1 - \frac{\omega^2}{z_2^2}) \quad \text{(it describes a notch)} && (4)\\
&\times(1 - \frac{\omega^2}{z_3^2}) && (5)\\
&\times(1 - \frac{\omega^2}{z_4^2}) && (6)\\
D(w) &= (1 - \mathrm{j}\frac{\omega}{p_1}) && (7)\\
&\times(1 - \frac{\omega^2 - \mathrm{j} \times 2p_2\omega}{p_2^2 + p_3^2}) && (8)\\
&\times(1 - \frac{\omega^2 + \mathrm{j} \times 2p_4\omega}{p_4^2 + p_5^2}) && (9)\\
&\times(1 - \frac{\omega^2 + \mathrm{j} \times 2p_6\omega}{p_6^2 + p_7^2}) && (10)\\
&\times(1 - \mathrm{j}\frac{\omega}{p_8}) && (11)
\end{aligned}$$

[7] They have been given by Alberto Gennai.